# This is the preprint of the contribution published as:

Zheng, Z., Wang, X., Flügge, J., **Nagel, T.** (2025): A stochastic modeling framework for radionuclide migration from deep geological repositories considering spatial variability *Adv. Water Resour.* **203**, art. 105003

# The publisher's version is available at:

https://doi.org/10.1016/j.advwatres.2025.105003

# Highlights

A stochastic modeling framework for radionuclide migration from deep geological repositories considering spatial variability

Zhibao Zheng, Xuerui Wang, Judith Flügge, Thomas Nagel

- An efficient stochastic framework for radionuclide migration is developed.
- The coupled stochastic Darcy and mass transport equations are solved numerically.
- A time-parallel algorithm is proposed to speed up long-duration stochastic simulations.
- The proposed framework is capable of handling high-dimensional random inputs.

# A stochastic modeling framework for radionuclide migration from deep geological repositories considering spatial variability

Zhibao Zheng<sup>a</sup>, Xuerui Wang<sup>b,\*</sup>, Judith Flügge<sup>b</sup>, Thomas Nagel<sup>c,d</sup>

#### **Abstract**

Considering the influence of uncertainties on radionuclide migration from deep geological repositories (DGR) is of great significance for safety assessment. However, stochastic modeling for DGR safety assessment remains challenging due to the high computational requirements of handling large regional scale models with multiphysics coupling, high-dimensional random inputs, and long simulated durations. This article introduces an efficient numerical framework to tackle this set of challenges. Specifically, the proposed framework relies on three key components, including efficient solutions of stochastic Darcy equations, propagation of stochastic quantities, and efficient solutions of stochastic mass transport equations. Unknown stochastic solutions are approximated by summing a series of products involving random variables and deterministic components. Alternating iterative algorithms are then proposed to decouple the original stochastic problems into deterministic equations for the spatial components, one-dimensional stochastic algebraic equations for the random variables, and one-dimensional ordinary differential equations for the temporal components. These deterministic equations can be solved efficiently using existing solvers, allowing the handling of large-scale problems. The one-dimensional stochastic algebraic equations can be solved efficiently using a sampling strategy, allowing the handling of high-dimensional stochastic state spaces. The one-dimensional ordinary differential equations can be solved cheaply and further accelerated using a time-parallel algorithm, allowing the handling

<sup>&</sup>lt;sup>a</sup>Leibniz Universität Hannover, Institute of Mechanics and Computational Mechanics, Appelstraße 9a, Hannover, 30167, Germany

<sup>&</sup>lt;sup>b</sup>Gesellschaft für Anlagen- und Reaktorsicherheit (GRS) gGmbH, Theodor-Heuss-Straße 4, Braunschweig, 38122, Germany

<sup>&</sup>lt;sup>c</sup>Technische Universität Bergakademie, Geotechnical Institute, Freiberg, Gustav-Zeuner-Straße 1, Freiberg, 09599, Germany

<sup>&</sup>lt;sup>d</sup>Hemholtz Centre for Environmental Research GmbH (UFZ), Department of Environmental Informatics, Permoserstr. 15, Leipzig, 04318, Germany

of long simulated time scales. Furthermore, a similar solution approximation and iterative algorithm are also used to propagate stochastic quantities from stochastic Darcy flow to stochastic mass transport. Numerical examples with up to 122 random variables and a simulated duration of one million years demonstrate the promising performance of the proposed framework. The numerical results demonstrate that the developed stochastic framework achieves accuracy comparable to Monte Carlo simulations while significantly improving computational efficiency by two orders of magnitude. Moreover, the evolutionary probability density functions obtained from our stochastic simulations indicate that the proposed framework could potentially serve as an efficient and robust tool for DGR risk assessment.

Keywords: Uncertainty modeling, Stochastic Darcy flow, Stochastic mass transport,

High-dimensional random inputs, Stochastic finite element method

#### 1. Introduction

Crystalline rock is widely considered one of the most suitable host rocks for a deep geological repository (DGR) for high-level nuclear waste (HLW), due to its low-permeability that restricts groundwater flow and reduces the potential for radionuclide migration. The safety assessment (SA) of such repositories rely critically on the accurate prediction of radionuclide migration over long timescales, often extending up to a million years [1], and the systematic consideration of relevant uncertainties [2]. In this context, numerical modeling plays a crucial role in characterizing the long-term transport properties of radionuclides, providing essential insights for safety evaluations. However, modeling radionuclide transport in crystalline rock is particularly challenging due to the presence of fractures and the associated significant uncertainties [3, 4, 5]. Due to their stochastic nature, fracture networks are usually difficult to characterize and introduce a high degree of spatial heterogeneity and variability, making it difficult to accurately predict transport pathways and rates. Recently, a great deal of modeling work has been conducted based on various approaches to characterize the complex flow and transport properties in fractured rocks. Typically,

\*Corresponding author

Email address: xuerui.wang@grs.de(Xuerui Wang)

Preprint submitted to Journal

February 23, 2025

four modeling approaches are used to address the impacts of fractures on flow and transport behavior in fractured rocks, namely, discrete fracture network (DFN), channel network (CN), equivalent porous medium model (EPM) and stochastic continuum model (SCM) approaches [6, 7]. In [6], a comparative study of groundwater flow modeling in fractured rocks was performed using the SCM, DFN, and CN approaches. The results demonstrate that these three modeling approaches yield similar mean values for the migration parameters. In particular, the SCM was found to effectively capture the advective flow properties of groundwater in various graphical representations. Compared to other numerical approaches, the SCM approach has significant advantages in terms of reducing computational effort due to its continuum-based formulation. It does not emphasize detailed geometric fracture data, but relies primarily on the results of hydraulic tests. Therefore, the SC approach provides a robust foundation for quantifying uncertainties in groundwater flow through fractures of varying distributions and scales.

In the present study, we develop a robust and computationally efficient stochastic modeling framework for the migration process of radionuclides from deep geological repositories in fractured rocks. Specifically, to capture variations in fracture properties and induced heterogeneity in space, the most relevant parameter governing migration, permeability, is modeled by spatially variable but continuous random fields within the SC framework. The stochastic mass transport equation governs radionuclide movement in groundwater flow, influenced by advection, dispersion, diffusion, sorption and decay. Groundwater flow, described by the stochastic Darcy equation, drives radionuclide transport and propagates uncertainties in geological parameters into the radionuclide concentration dynamics. Therefore, the key to simulating radionuclide migration is to solve the stochastic multiphysics problem of Darcy flow coupled with radionuclide mass transport, which typically involves large regional scales, high-dimensional random inputs and long time frame. Since the stochastic Darcy flow and the stochastic mass transport are uni-laterally coupled in a sequential way, where the stochastic solution of mass transport relies on the stochastic solution of Darcy flow, the challenge lies on the efficient solution of stochastic "single-physical" problems (i.e., uncoupled Darcy flow and mass transport) and the propagation of stochastic quantities between Darcy flow and mass transport.

For the first challenge, several methods originally developed for stochastic uncoupled problems

have been extended to solve each component of the stochastic coupled case. Monte Carlo simulation (MCS) and its extensions [8, 9] are widely used because of their broad applicability. Such methods have the attractive advantages of being easily implemented using existing deterministic multiphysics solvers and being suitable for handling high-dimensional random inputs. However, a large number of deterministic simulations of mass transport coupled with Darcy flow need to be solved to achieve high-accuracy stochastic solutions, which is prohibitively expensive for the large-scale and long-duration stochastic problems considered in this article [10]. Another popular method is based on the polynomial chaos (PC) expansion [11, 12]. This method uses (generalized) PC bases to approximate stochastic solutions [13, 14]. The original stochastic Darcy and mass transport problems are then transformed into augmented deterministic Darcy and mass transport equations using the stochastic Galerkin method. However, since the size of the augmented deterministic problems increases dramatically as the number of random variables and/or the PC basis truncation order increases, the PC-based approximation is susceptible to the curse of dimensionality, which makes large-scale and/or high-dimensional stochastic analyses prohibitively expensive in many cases of practical relevance. Therefore, the computational efficiency of PC-based methods needs to be further improved. Furthermore, other methods, such as the multi-fidelity method, the response surface method and machine learning-based methods [15, 16, 17, 18], have also been developed to solve each component of stochastic multiphysics problems. Their computational accuracy and efficiency need to be further improved to adapt to stochastic multiphysics analysis. For the second difficulty, existing studies usually use the PC approximation of the stochastic solution of each physical field to exchange probabilistic information between different physical fields [19, 20, 21, 22]. In addition to the above difficulties faced by PC-based approximations, probabilistic information transferred between different physical fields must be assumed to be lowdimensional and then approximated by Karhunen-Loève expansion or reduced-dimensional PC expansion [19, 21]. Currently, more efficient methods are still needed to propagate the highdimensional probabilistic information arising from the complex stochastic multiphysics analysis considered in this study.

To address the above challenges and achieve efficient simulation of stochastic radionuclide migration processes, the contribution of this article relies on three aspects, including efficient

solutions of stochastic Darcy flow and stochastic mass transport, and effective probabilistic information propagation from Darcy flow to radionuclide mass transport. The first contribution is concentrated on an efficient solution algorithm for high-dimensional stochastic Darcy equations. Specifically, a stochastic solution approximation is used to decouple the unknown stochastic solution as a summation of a series of products of random variables and deterministic spatial vectors. An alternating iterative algorithm combined with stochastic and deterministic Galerkin methods [13, 14, 23] is then used to transform the original stochastic Darcy problem into deterministic equations about the spatial vectors and one-dimensional stochastic algebraic equations about the random variables. The deterministic equations can be solved efficiently using existing solvers [24], even for very large-scale problems. Moreover, one-dimensional stochastic algebraic equations are solved efficiently using a sample-based strategy [25, 26], which differs from existing tensor product constructions for such solution approximations within the framework of proper generalized decomposition methods [27, 28]. Benefiting from the dimensionality independence of random samples, the sample approximation of random variable components allows handling both low- and high-dimensional random inputs in a unified form, thereby significantly mitigating the curse of dimensionality caused by high-dimensional random inputs. The second contribution is to extend the above solution algorithm to solve stochastic mass transport equations for long durations. In this case, the unknown stochastic solution is approximated as a summation of a series of products of random variables, deterministic spatial vectors and deterministic temporal vectors. Similarly, the original stochastic mass transport problem is transformed into deterministic equations about the spatial vectors, one-dimensional stochastic algebraic equations about the random variables, and one-dimensional ordinary differential equations about the temporal vectors. The first two equations are solved in a similar way as described above, and the one-dimensional ordinary differential equations are solved cheaply and can be further accelerated using a time-parallel algorithm. Therefore, the long time scales relevant in nuclear waste disposal can be handled very well. The third contribution is to efficiently propagate stochastic quantities (e.g. stochastic velocities) from Darcy flow to mass transport. This typically involves high-dimensional probabilistic propagation. Similarly to the above algorithms, the stochastic quantities are approximated using decoupled forms consisting of deterministic vectors and random variables. These components

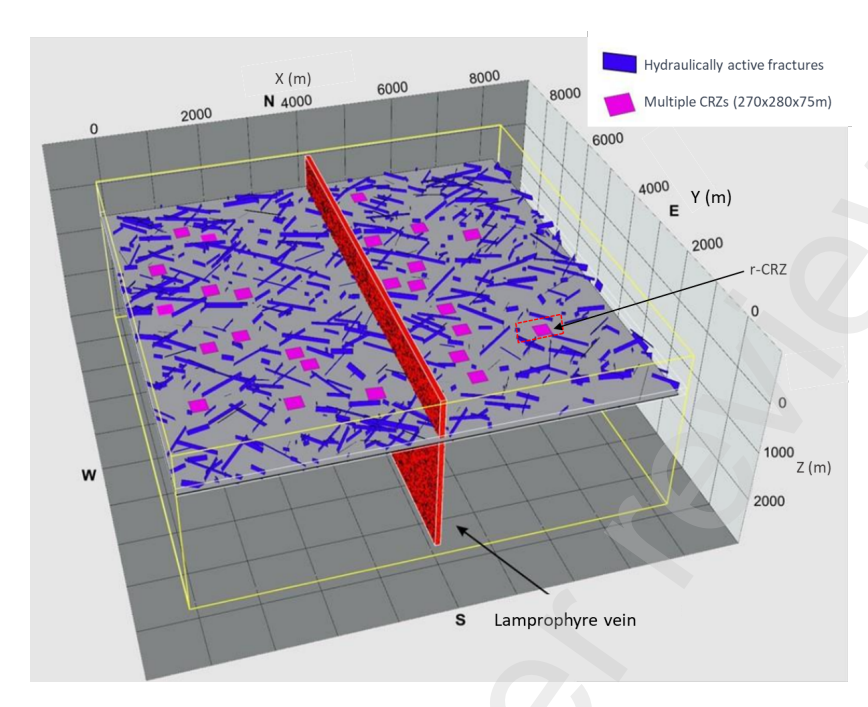
are solved using an alternating iterative scheme similar to the above algorithms but simpler. The promising performance of the proposed framework is demonstrated through numerical examples with up to 122 random variables, 60 000 degree of freedoms (DoFs) and a simulation duration of one million years.

This article is organized as follows: The basic problem of radionuclide migration from deep geological repositories with uncertainties due to spatial variability of key physical properties and the corresponding stochastic finite element equations are presented in Section 2. The solution algorithms are proposed in Section 3, including the stochastic solution approximation, the iterative algorithm, and the time-parallel strategy. Afterward, detailed algorithm implementations are given in Section 4. In Section 5, numerical examples with high-dimensional random inputs and long durations are investigated to demonstrate the promising performance of the proposed framework. Section 6 closes the paper with discussions and conclusions.

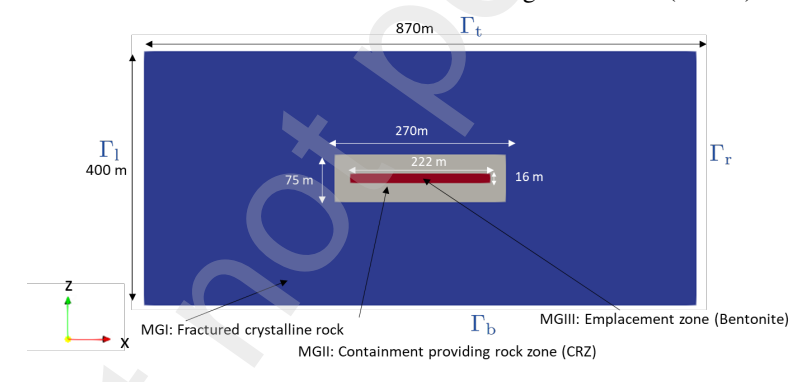
## 2. Stochastic continuum representation of transport in fracture and matrix

#### 2.1. Model description

In this study, we investigate the Modified Multiple Containment Providing Rock Zones (mmCRZs) concept (Fig. 1a), which is proposed as a potential repository concept for a deep geological repository (DGR) in crystalline rock in Germany [29]. This concept assumes the presence of several discrete intact rock zones with low permeability within the crystalline host rock, which serve as an effective geological barrier to prevent the migration of radionuclides into the biosphere. These intact rock zones are isolated from each other by surrounding fractured rock zones. Individual emplacement areas of nuclear waste are constructed in each of these intact rock zones. To further enhance repository safety, an engineered barrier system (EBS) is integrated into the design, incorporating bentonite buffer material placed around the waste canisters [30]. To conduct a detailed analysis of the flow and transport behavior of the radionuclides in the near field of the repository, our modeling considers a two-dimensional section of a reference containment providing rock zone (r-CRZ) with its surrounding fractured rocks from the m-mCRZs. Consistent with the repository concept, the model domain is divided into three material groups (Fig. 1b): the



(a) Schematic illustration of the repository concept for the modified Multiple Containment-Providing Rock Zone (m-mCRZ) repository concept [29], and the considered reference Containment-Providing Rock Zone (r-CRZ).



(b) Model geometry, material groups and boundaries for the r-CRZ.

Figure 1: Repository concept and simulation domain.

emplacement zone containing nuclear waste (Material Group III, MG III), the intact containment providing rock zone (CRZ) (Material Group II, MG II), and the fractured crystalline rock (Material Group I, MG I). The goal is to model the migration of radionuclides away from the emplacement area.

## 2.2. Mathematical model for flow and transport

Our modeling framework adopts the stochastic continuum approach, treating the fractured rock mass as a continuum with spatially variable properties. The flow and mass transport processes within the fractured rocks are assumed to be similar to those through porous media [31]. The fractured rock mass is thus represented as a locally averaged homogeneous equivalent porous medium (EPM). In this equivalent system, the heterogeneity introduced by fractures and fracture networks is captured through spatially random distributions of hydraulic property parameters. Specifically, in our model a spatially random distribution of element permeability is employed to represent the locally averaged properties, which can effectively account for the inherent spatial variability in the fractured rock system. The radionuclide transport (RNT) is primarily governed by advective groundwater flow, diffusion, hydrodynamic dispersion, sorption, and decay.

#### 2.2.1. Continuity equation

The groundwater flow is described by the continuity equation, which is derived based on the mass balance of the liquid phase in the porous media

$$\frac{\partial (\phi \rho)}{\partial t} = -\nabla \cdot (\phi \rho \mathbf{v}) + Q^{\mathbf{w}},\tag{1}$$

where  $\phi$  is the porosity, which has different values for MG I, MG II and MG III,  $Q^w$  is a source/sink flow rate,  $\rho$  is the density of pore fluid, and  $v \in \mathbb{R}^2$  is the vector of flow velocity in the two-dimensional domain considered here. In our simulation, we assume the use of Darcy's law to describe the flow process, where the Darcy velocity q is given by

$$\boldsymbol{q} = \phi \boldsymbol{v} = -\frac{\widehat{\boldsymbol{K}}}{\mu} \cdot (\nabla p - \rho \boldsymbol{g}) \in \mathbb{R}^2, \tag{2}$$

where  $\widehat{K} = K\mathbf{I}_2 \in \mathbb{R}^{2\times 2}$  denotes the isotropic permeability tensor, K is a (spatially inhomogeneous) scalar function,  $\mathbf{I}_2 \in \mathbb{R}^{2\times 2}$  is the identity tensor,  $\mu$  is the liquid viscosity,  $\mathbf{g} \in \mathbb{R}^2$  is the gravitational acceleration vector, and p is the pore water pressure. In this article, we only consider isotropic permeability, but  $\widehat{K}$  can be anisotropic in general. In practice, aside from the permeability  $\widehat{K}$ , other parameters can also be modeled as random inputs, be it as random variables or as random fields. In this study, without loss of generality, we only consider that the scalar function K is modeled as

a random field  $K(\mathbf{x}, \theta)$ , where  $\mathbf{x} = [x, z]^{\mathrm{T}} \in \mathbb{R}^2$  is the spatial placement vector with the coordinate system introduced in Fig. 1b. The random event  $\theta \in \Theta$  is defined in a suitable probability space  $(\Theta, \Xi, \mathcal{P})$ , where  $\Theta$  denotes the space of elementary events,  $\Xi$  is the  $\sigma$ -algebra defined on  $\Theta$ , and  $\mathcal{P}$  is the probability measure. Substituting Eq. (2) in Eq. (1), the stochastic governing equation for porous media flow with the pore pressure p as primary variable can be derived

$$\left(\phi \frac{\partial \rho}{\partial p} + \rho \frac{\partial \phi}{\partial p}\right) \frac{\partial p\left(t, \mathbf{x}, \theta\right)}{\partial t} = \nabla \cdot \left[\rho \frac{\widehat{K}\left(\mathbf{x}, \theta\right)}{\mu} \cdot \left[\nabla p\left(t, \mathbf{x}, \theta\right) - \rho \mathbf{g}\right]\right] + Q^{w},\tag{3}$$

Considering the steady-state flow regime of Eq. (3) and the isotropic random permeability tensor  $\widehat{K}(\mathbf{x}, \theta) = K(\mathbf{x}, \theta) \mathbf{I}_2$ , the weak form of Eq. (3) is given by

$$\int_{\Omega} \rho \, \frac{K(\theta)}{\mu} \nabla p(\theta) \cdot \nabla \eta \, d\Omega - \int_{\Omega} \rho^2 \, \frac{K(\theta)}{\mu} \mathbf{g} \cdot \nabla \eta \, d\Omega + \int_{\Omega} Q^{\mathsf{w}} \eta \, d\Omega = 0. \tag{4}$$

where the dependence on placement  $\mathbf{x}$  is omitted here, and  $\eta$  is the deterministic spatial test function with  $\eta|_{\partial\Omega} = 0^1$ .

## 2.2.2. Mass transport equation for radionuclide migration

Furthermore, for the radionuclide migration, we consider the following stochastic mass transport equation of a representative species

$$\frac{\partial}{\partial t} \left[ \phi RC(t, \theta) \right] = \nabla \cdot \left[ \phi \mathbf{D}(\theta) \cdot \nabla C(t, \theta) \right] - \mathbf{q}(\theta) \cdot \nabla C(t, \theta) - \phi R\tau C(t, \theta)$$
(5)

with specific initial concentration  $C(0,\theta)$ , where  $C(t,\theta)$  represents the time-dependent stochastic concentration of the radionuclide, the coefficient  $\boldsymbol{D}(\theta) \in \mathbb{R}^{2\times 2}$  is known as the diffusion-dispersion tensor consisting of molecular diffusion  $\boldsymbol{D}_{\mathrm{f}} \in \mathbb{R}^{2\times 2}$  and mechanical dispersion  $\boldsymbol{D}_{\mathrm{p}}(\theta) \in \mathbb{R}^{2\times 2}$ 

$$\boldsymbol{D}(\theta) = \boldsymbol{D}_{f} + \boldsymbol{D}_{p}(\theta). \tag{6}$$

In our modeling,  $D_f = D_f \mathbf{I}_2$  is considered to be isotropic, where  $D_f$  is a scalar value (or a spatial function). The mechanical dispersion is given by the dispersion matrix

$$\boldsymbol{D}_{p}(\theta) = (\alpha_{L} - \alpha_{T}) \frac{\boldsymbol{v} \otimes \boldsymbol{v}}{\|\boldsymbol{v}\|} + \alpha_{T} \|\boldsymbol{v}\| \boldsymbol{I}_{2}, \tag{7}$$

 $<sup>^1</sup>$ Without loss of generality, Dirichlet conditions on the entire boundary  $\partial\Omega$  were considered in Eq. (4).

where  $\alpha_L$  and  $\alpha_T$  are the longitudinal and transversal dispersion coefficients, respectively, and  $\|\cdot\|$  represents the magnitude of the vector. Furthermore, the coefficient R is the retardation factor defined as

$$R = 1 + \rho_{\rm b} k_{\rm d} / \phi, \tag{8}$$

where  $k_d$  is the sorption coefficient of the radionuclides,  $\tau = \ln 2/t_{1/2}$  is the first-order decay constant,  $\rho_b$  is the bulk density of the porous medium, and  $t_{1/2}$  is the half life of the radionuclide. Similar to Eq. (4), the weak form of Eq. (5) under prescribed boundary concentrations is given by

$$\frac{\partial}{\partial t} \int_{\Omega} \phi RC(t,\theta) \zeta \, d\Omega + \int_{\Omega} \phi \mathbf{D}(\theta) \cdot \nabla C(t,\theta) \cdot \nabla \zeta \, d\Omega + \int_{\Omega} \mathbf{q}(\mathbf{x},\theta) \cdot \nabla C(t,\theta) \zeta \, d\Omega + \int_{\Omega} \phi R\tau \, C(t,\theta) \zeta \, d\Omega = 0, \tag{9}$$

where  $\zeta$  is the spatial test function with  $\zeta|_{\partial\Omega} = 0$ .

#### 2.3. Modeling of random fields

In this article, we assume that the permeability-related scale function  $K(\mathbf{x}, \theta)$  is a Gaussian random field. For general non-Gaussian random fields, some advanced simulation methods can be used, e.g., [32, 33, 34]. Specifically, the Gaussian random field  $K(\mathbf{x}, \theta)$  has the mean value  $K_0(\mathbf{x})$  and the covariance function

$$\operatorname{Cov}_{K}(\mathbf{x}_{1}, \mathbf{x}_{2}) = \sigma_{K}^{2} \exp\left(-\frac{|\mathbf{x}_{1} - \mathbf{x}_{2}|}{l_{\mathbf{x}}}\right), \tag{10}$$

where  $\sigma_K$  is the standard deviation and  $l_x$  is the correlation length. By using the Karhunen-Loève expansion [13, 35], the random field  $K(\mathbf{x}, \theta)$  can be approximated as

$$K(\mathbf{x}, \theta) = K_0(\mathbf{x}) + \sum_{i=1}^{r_K} \xi_i(\theta) \sqrt{\kappa_i} K_i(\mathbf{x}), \qquad (11)$$

where  $\{\xi_i(\theta)\}_{i=1}^{r_K}$  are a set of mutually independent standard Gaussian random variables, and  $\{\kappa_i, K_i(\mathbf{x})\}_{i=1}^{r_K}$  are respectively the eigenvalues and eigenvectors of the covariance function  $\text{Cov}_K(\mathbf{x}_1, \mathbf{x}_2)$ . They are solved by the following Fredholm integral equation of the second kind

$$\int_{\Omega} \operatorname{Cov}_{K}(\mathbf{x}_{1}, \mathbf{x}_{2}) K_{i}(\mathbf{x}_{2}) d\mathbf{x}_{2} = \kappa_{i} K_{i}(\mathbf{x}_{1}), \qquad (12)$$

which can be solved efficiently using existing eigenvalue solvers [36], even for very large-scale problems.

#### 2.4. Stochastic finite element equations

#### 2.4.1. Stochastic finite element equation for stochastic Darcy flow

Applying finite element discretization to the weak form (4), we can generate the following stochastic finite element equation (SFEE)

$$\mathbf{A}(\theta)\,\mathbf{p}(\theta) = \mathbf{B}(\theta)\,,\tag{13}$$

where  $\mathbf{p}(\theta) \in \mathbb{R}^n$  is the unknown stochastic nodal solution of pressure, n is the total number of degrees of freedom (DoFs), the stochastic matrix  $\mathbf{A}(\theta) = \bigcup_{e=1}^{n_e} \mathbf{A}^{(e)}(\theta) \in \mathbb{R}^{n \times n}$  is obtained by assembling all stochastic element matrices, and the stochastic vector  $\mathbf{B}(\theta) = \bigcup_{e=1}^{n_e} \mathbf{B}^{(e)}(\theta) \in \mathbb{R}^n$  is obtained by assembling all stochastic element vectors. Taking the linear triangle element as an example, the stochastic solution of each element is approximated as

$$p^{(e)}(\theta) = \mathbf{N}\mathbf{p}^{(e)}(\theta) \in \mathbb{R},\tag{14}$$

where  $\mathbf{p}^{(e)}(\theta) = \left[p_1^{(e)}(\theta), p_2^{(e)}(\theta), p_3^{(e)}(\theta)\right]^T \in \mathbb{R}^3$  is the vector of nodal pressure values, and the shape function matrix  $\mathbf{N}$  and its derivative  $\frac{\partial \mathbf{N}}{\partial \mathbf{x}}$  are

$$\mathbf{N} = \begin{bmatrix} N_1 & N_2 & N_3 \end{bmatrix} \in \mathbb{R}^{1 \times 3}, \quad \frac{\partial \mathbf{N}}{\partial \mathbf{x}} = \begin{bmatrix} \frac{\partial N_1}{\partial x} & \frac{\partial N_2}{\partial x} & \frac{\partial N_3}{\partial x} \\ \frac{\partial N_1}{\partial z} & \frac{\partial N_2}{\partial z} & \frac{\partial N_3}{\partial z} \end{bmatrix} \in \mathbb{R}^{2 \times 3}.$$
 (15)

According to Eq. (4), the stochastic element matrix  $\mathbf{A}^{(e)}(\theta)$  and the stochastic element vector  $\mathbf{B}^{(e)}(\theta)$  are given by

$$\mathbf{A}^{(e)}(\theta) = \int_{\Omega^{(e)}} \rho \, \frac{K(\theta)}{\mu} \left( \frac{\partial \mathbf{N}}{\partial \mathbf{x}} \right)^{\mathrm{T}} \frac{\partial \mathbf{N}}{\partial \mathbf{x}} \, \mathrm{d}\Omega^{(e)} \in \mathbb{R}^{3 \times 3}, \quad \mathbf{B}^{(e)} = \int_{\Omega^{(e)}} \left[ \rho^2 \, \frac{K(\theta)}{\mu} \left( \frac{\partial \mathbf{N}}{\partial \mathbf{x}} \right)^{\mathrm{T}} \mathbf{g} - \mathbf{N}^{\mathrm{T}} Q^{\mathrm{w}} \right] \mathrm{d}\Omega^{(e)} \in \mathbb{R}^3. \tag{16}$$

In a similar way, other types and higher-order elements can be used for the spatial discretization. In addition, considering the random field approximation (11), the stochastic matrix  $\mathbf{A}(\theta)$  and the stochastic vector  $\mathbf{B}(\theta)$  in Eq. (13) can be further expressed as

$$\mathbf{A}(\theta) = \sum_{j=0}^{r_K} \xi_j(\theta) \mathbf{A}_j, \quad \mathbf{B}(\theta) = \sum_{j=0}^{r_K} \xi_j(\theta) \mathbf{B}_j,$$
 (17)

where  $\xi_0(\theta) \equiv 0$  and the deterministic matrices and vectors  $\{\mathbf{A}_j \in \mathbb{R}^{n \times n}, \mathbf{B}_j \in \mathbb{R}^n\}_{j=0}^{r_K}$  are obtained by assembling the following deterministic element matrices and vectors for the example of the linear triangular element

$$\mathbf{A}_{0}^{(e)} = \int_{\Omega^{(e)}} \rho \, \frac{K_{0}}{\mu} \left( \frac{\partial \mathbf{N}}{\partial \mathbf{x}} \right)^{T} \frac{\partial \mathbf{N}}{\partial \mathbf{x}} \, d\Omega^{(e)} \in \mathbb{R}^{3 \times 3}, \quad \mathbf{B}_{0}^{(e)} = \int_{\Omega^{(e)}} \left[ \rho^{2} \, \frac{K_{0}}{\mu} \left( \frac{\partial \mathbf{N}}{\partial \mathbf{x}} \right)^{T} \mathbf{g} - \mathbf{N}^{T} Q^{w} \right] d\Omega^{(e)} \in \mathbb{R}^{3}, \tag{18a}$$

$$\mathbf{A}_{j}^{(e)} = \int_{\Omega^{(e)}} \rho \, \frac{\sqrt{\kappa_{i}} K_{j}}{\mu} \left( \frac{\partial \mathbf{N}}{\partial \mathbf{x}} \right)^{\mathrm{T}} \frac{\partial \mathbf{N}}{\partial \mathbf{x}} \, \mathrm{d}\Omega^{(e)} \in \mathbb{R}^{3 \times 3}, \quad \mathbf{B}_{j}^{(e)} = \int_{\Omega^{(e)}} \rho^{2} \, \frac{\sqrt{\kappa_{i}} K_{j}}{\mu} \left( \frac{\partial \mathbf{N}}{\partial \mathbf{x}} \right)^{\mathrm{T}} \mathbf{g} \, \mathrm{d}\Omega^{(e)} \in \mathbb{R}^{3}, \ \forall j \in \{1, r\}.$$

$$(18b)$$

There are several difficulties in solving Eq. (13). One the one hand, large-scale problems typically result in a large number of spatial DoFs, whose solutions are time-consuming and storage-intensive. On the other hand, high-dimensional random inputs, e.g., a large truncation number r in Eq. (11), suffer from the so-called curse of dimensionality in stochastic spaces. The coupling of large scales and high stochastic dimensions will make the solution more difficult. To address these issues, we will present an efficient and accurate algorithm in the next section.

#### 2.4.2. Stochastic finite element equation for stochastic mass transport

With the stochastic pressure obtained by Eq. (13), the stochastic velocity vector  $\mathbf{v}(\theta)$  and the stochastic diffusion-dispersion matrix  $\mathbf{D}(\theta)$  can be calculated using Eqs. (2) and (7). Similar to Eq. (13), applying finite element discretization to the weak form (9), we can generate the following SFEE

$$\mathbf{M}\frac{\partial \mathbf{C}(t,\theta)}{\partial t} + \mathbf{Z}(\theta)\mathbf{C}(t,\theta) = \mathbf{0},\tag{19}$$

where  $\mathbf{C}(t,\theta) \in \mathbb{R}^n$  is the time-dependent stochastic nodal solution of concentration, the matrices  $\mathbf{M} = \bigcup_{e=1}^{n_e} \mathbf{M}^{(e)} \in \mathbb{R}^{n \times n}$  and  $\mathbf{Z}(\theta) = \bigcup_{e=1}^{n_e} \mathbf{Z}^{(e)}(\theta) \in \mathbb{R}^{n \times n}$  are obtained by assembling all stochastic element matrices. Considering again the linear triangle element, we have

$$\mathbf{M}^{(e)} = \int_{\Omega^{(e)}} \phi R \, \mathbf{N}^{T} \mathbf{N} \, d\Omega^{(e)} \in \mathbb{R}^{3 \times 3}, \tag{20a}$$

$$\mathbf{Z}^{(e)} (\theta) = \int_{\Omega^{(e)}} \phi \left(\frac{\partial \mathbf{N}}{\partial \mathbf{x}}\right)^{T} \mathbf{D} (\theta) \, \frac{\partial \mathbf{N}}{\partial \mathbf{x}} \, d\Omega^{(e)} + \int_{\Omega^{(e)}} \phi \, \mathbf{N}^{T} \mathbf{v}^{T} (\theta) \, \frac{\partial \mathbf{N}}{\partial \mathbf{x}} \, d\Omega^{(e)} + \int_{\Omega^{(e)}} \phi R \tau \, \mathbf{N}^{T} \mathbf{N} \, d\Omega^{(e)} \in \mathbb{R}^{3 \times 3}, \tag{20b}$$

where  $\mathbf{D}(\theta) \in \mathbb{R}^{2\times 2}$  is the matrix form of  $\mathbf{D}(\theta)$  at each integration point, and  $\mathbf{v}(\theta) \in \mathbb{R}^2$  is the vector form of  $\mathbf{v}(\theta)$  at integration point. It is noted that the matrix  $\mathbf{M}$  is deterministic and only  $\mathbf{Z}(\theta)$  is an asymmetric stochastic matrix. Furthermore, following the expansion Eq. (11), we assume that the stochastic velocity  $\mathbf{v}(\theta)$  and the stochastic diffusion-dispersion tensor  $\mathbf{D}(\theta)$  have the following decoupled forms (this will be achieved later on)

$$\boldsymbol{v}(\theta) = \sum_{i=1}^{r_{\boldsymbol{v}}} \chi_{\boldsymbol{v},i}(\theta) \, \boldsymbol{v}_i, \quad \boldsymbol{D}(\theta) = \sum_{j=1}^{r_D} \chi_{\boldsymbol{D},j}(\theta) \, \boldsymbol{D}_j, \tag{21}$$

where  $\{\chi_{\nu,i}(\theta)\}_{i=1}^{r_{\nu}}$  and  $\{\chi_{D,j}(\theta)\}_{j=1}^{r_{D}}$  are scalar random variables, and  $\{\nu_{i}\}_{i=1}^{r_{\nu}}$  and  $\{\boldsymbol{D}_{j}\}_{j=1}^{r_{D}}$  are deterministic components/bases. In this way, we can rewrite the SFEE (19) as

$$\mathbf{M} \frac{\partial \mathbf{C}(t,\theta)}{\partial t} + \left(\sum_{i=0}^{r_{\mathbf{Z}}} \chi_i(\theta) \mathbf{Z}_i\right) \mathbf{C}(t,\theta) = \mathbf{0}, \tag{22}$$

where  $r_{\mathbf{Z}} = r_{v} + r_{\mathbf{D}}$ , the random variables  $\chi_{i}(\theta) = \chi_{v,i}(\theta)$ ,  $i \in \{1, r_{v}\}$  and  $\chi_{r_{v}+j}(\theta) = \chi_{\mathbf{D},j}(\theta)$ ,  $j \in \{1, r_{\mathbf{D}}\}$ , and the deterministic element matrices of  $\mathbf{Z}_{i}$  are given by

$$\mathbf{Z}_0^{(e)} = \int_{\Omega^{(e)}} \phi R \tau \, \mathbf{N}^{\mathrm{T}} \mathbf{N} \, \mathrm{d}\Omega^{(e)} \in \mathbb{R}^{3 \times 3}, \tag{23a}$$

$$\mathbf{Z}_{i}^{(e)} = \int_{\Omega^{(e)}} \phi \, \mathbf{N}^{\mathrm{T}} \mathbf{v}_{i}^{\mathrm{T}} \frac{\partial \mathbf{N}}{\partial \mathbf{x}} \, \mathrm{d}\Omega^{(e)} \in \mathbb{R}^{3 \times 3}, \quad i \in \{1, r_{\nu}\},$$
(23b)

$$\mathbf{Z}_{r_{\nu}+j}^{(e)} = \int_{\Omega^{(e)}} \phi \left(\frac{\partial \mathbf{N}}{\partial \mathbf{x}}\right)^{\mathrm{T}} \mathbf{D}_{j} \frac{\partial \mathbf{N}}{\partial \mathbf{x}} d\Omega^{(e)} \in \mathbb{R}^{3\times 3}, \quad j \in \{1, r_{D}\},$$
 (23c)

In order to solve Eq. (19) efficiently and accurately, in addition to the difficulties of handling large scales and high-dimensional random inputs, long simulated time spans must also be considered in this study. To address long duration and its coupling with large scales and high stochastic dimensions, an efficient algorithm will be proposed in the next section. Furthermore, the stochastic velocity  $\mathbf{v}(\theta)$  and the stochastic diffusion-dispersion coefficient  $\mathbf{D}(\theta)$  need to be calculated based on the stochastic solution of Eq. (13) and are reused in Eq. (19). This is not trivial, as they typically involve high stochastic dimensions and need to be propagated to Eq. (19) with high accuracy. This is also a focus to be solved in the present study.

#### 3. Efficient solution algorithms for SFEEs

In this section we focus on developing efficient algorithms to solve the SFEEs (13) and (19) and to propagate stochastic quantities between them.

#### 3.1. Solution algorithm for SFEE of Darcy flow

To solve SFEE (13), we approximate the stochastic solution  $\mathbf{p}(\theta)$  using the following decoupled and greedy way

$$\mathbf{p}_{k}(\theta) = \sum_{i=1}^{k} \lambda_{i}(\theta) \, \mathbf{d}_{i} = \mathbf{p}_{k-1}(\theta) + \lambda_{k}(\theta) \, \mathbf{d}_{k}, \tag{24}$$

where  $\mathbf{p}_{k-1}(\theta) = \sum_{i=1}^{k-1} \lambda_i(\theta) \, \mathbf{d}_i \in \mathbb{R}^n$  and  $\mathbf{p}_k(\theta) \in \mathbb{R}^n$  are the  $(k-1)^{\text{th}}$  and  $k^{\text{th}}$  approximations of the stochastic solution. For the approximation, a set of random variables  $\{\lambda_i(\theta)\}_{i=1}^k$  and a set of deterministic vectors  $\{\mathbf{d}_i \in \mathbb{R}^n\}_{i=1}^k$  are used so that  $\lambda_k(\theta) \, \mathbf{d}_k \in \mathbb{R}^n$  is the  $k^{\text{th}}$  stochastic increment of the stochastic solution. In practice, both the random variables  $\{\lambda_i(\theta)\}_{i=1}^k$  and the deterministic vectors  $\{\mathbf{d}_i \in \mathbb{R}^n\}_{i=1}^k$  are not known a priori. We adopt an iterative method to solve the pair  $\{\lambda_i(\theta), \mathbf{d}_i\}$  one by one. To this end, substituting Eq. (24) into Eq. (13) and assuming that the approximation  $\mathbf{p}_{k-1}(\theta)$  has been known (or given as an initial value), Eq. (13) is rewritten as

$$\mathbf{A}(\theta)\,\lambda_k(\theta)\,\mathbf{d}_k = \mathbf{B}_k(\theta)\,,\tag{25}$$

where the vector  $\mathbf{B}_k(\theta) = \mathbf{B}(\theta) - \mathbf{A}(\theta) \mathbf{p}_{k-1}(\theta) \in \mathbb{R}^n$ . In this way, we only need to solve the  $k^{\text{th}}$  unknown pair  $\{\lambda_k(\theta), \mathbf{d}_k\}$ . The following alternating iteration is used for this:

For a known random variable  $\lambda_k(\theta)$  (or given an initial value), applying the stochastic Galerkin method [13, 14] to Eq. (25) we have

$$\mathbb{E}\left\{\lambda_{k}^{2}\left(\theta\right)\mathbf{A}\left(\theta\right)\right\}\mathbf{d}_{k}=\mathbb{E}\left\{\lambda_{k}\left(\theta\right)\mathbf{B}_{k}\left(\theta\right)\right\},\tag{26}$$

where the expectation operator  $\mathbb{E} \{\cdot\} = \int_{\Theta} \cdot d\mathcal{P}(\theta)$ . Eq. (26) is a linear deterministic equation for the unknown vector  $\mathbf{d}_k$ , which can be solved efficiently and accurately by existing numerical solvers [24], even for very large problems. In the practical implementation, to speed up the convergence, we let  $\mathbf{d}_k$  be orthogonal to the previously obtained vectors  $\{\mathbf{d}_i\}_{i=1}^{k-1}$ . The following Gram-Schmidt orthonormalization process is used for this

$$\mathbf{d}_{k} = \mathbf{d}_{k} - \sum_{i=1}^{k-1} \frac{\mathbf{d}_{k}^{\mathrm{T}} \mathbf{d}_{i}}{\mathbf{d}_{i}^{\mathrm{T}} \mathbf{d}_{i}} \mathbf{d}_{i} = \mathbf{d}_{k} - \sum_{i=1}^{k-1} \left( \mathbf{d}_{k}^{\mathrm{T}} \mathbf{d}_{i} \right) \mathbf{d}_{i}, \quad \mathbf{d}_{k}^{\mathrm{T}} \mathbf{d}_{k} = 1,$$
(27)

which is equivalent to  $\mathbf{d}_k^{\mathrm{T}} \mathbf{d}_i = \delta_{ki}, i \in \{1, k-1\}$ , where  $\delta_{ki}$  is the Kronecker delta.

Based on the obtained vector  $\mathbf{d}_k$  using Eq. (26), applying the classical Galerkin method to Eq. (25) we have<sup>2</sup>

$$a_k(\theta) \lambda_k(\theta) = b_k(\theta),$$
 (28)

where the scalar random variables  $a_k(\theta) \in \mathbb{R}$  and  $b_k(\theta) \in \mathbb{R}$  are given by

$$a_k(\theta) = \mathbf{d}_k^{\mathrm{T}} \mathbf{A}(\theta) \mathbf{d}_k, \quad b_k(\theta) = \mathbf{d}_k^{\mathrm{T}} \mathbf{B}_k(\theta).$$
 (29)

Although Eq. (28) has a very simple form, it still suffers from the curse of dimensionality occurring in high-dimensional stochastic spaces if common numerical methods are used, such as the PC expansion-based methods. To avoid this, we adopt a sampling method to solve Eq. (28), which corresponds to

$$\lambda_k(\widehat{\boldsymbol{\theta}}) = a_k(\widehat{\boldsymbol{\theta}}) \oslash b_k(\widehat{\boldsymbol{\theta}}) \in \mathbb{R}^{n_s}, \tag{30}$$

where  $\lambda_k(\widehat{\theta}) \in \mathbb{R}^{n_s}$ ,  $a_k(\widehat{\theta}) \in \mathbb{R}^{n_s}$  and  $b_k(\widehat{\theta}) \in \mathbb{R}^{n_s}$  are the sample realization vectors of the random variables  $\lambda_k(\theta)$ ,  $a_k(\theta)$  and  $b_k(\theta)$ , respectively, and  $\emptyset$  is the element-wise division of two vectors. Since all random inputs are embedded into random sample vectors, Eq. (30) is insensitive to the stochastic dimension and cheap enough even for very high-dimensional random inputs. In this sense, the proposed method avoids the curse of dimensionality to a great extent. The effectiveness of this strategy has been verified in our previous studies [25, 26].

Repeatedly solving Eqs. (25) and (30) until both the random variable  $\lambda_k(\theta)$  and the deterministic vector  $\mathbf{d}_k$  converge, we can obtain their final solutions. The next pair  $\{\lambda_{k+1}(\theta), \mathbf{d}_{k+1}\}$  is solved in the same way. By solving enough pairs until a certain accuracy is reached, we can obtain the final stochastic solution of  $\mathbf{p}(\theta)$ . However, it is important to note that each pair is solved in a greedy way and the random variables are approximated using random samples, which may not be accurate enough in some cases. To address this, we consider  $\mathbf{Q} = [\mathbf{d}_1, \dots, \mathbf{d}_k] \in \mathbb{R}^{n \times k}$  as a set of reduced bases and re-approximate the stochastic solution as  $\mathbf{p}(\theta) = \mathbf{Q}\mathbf{\Lambda}(\theta)$ , where the random variable vector  $\mathbf{\Lambda}(\theta) = [\lambda_1(\theta), \dots, \lambda_k(\theta)]^T \in \mathbb{R}^k$  was introduced. To improve the computational accuracy of the stochastic solution, the following reduced-order SFEE is used to recalculate  $\mathbf{\Lambda}(\theta)$ 

$$\left[\mathbf{Q}^{\mathrm{T}}\mathbf{A}\left(\theta\right)\mathbf{Q}\right]\mathbf{\Lambda}\left(\theta\right) = \mathbf{Q}^{\mathrm{T}}\mathbf{B}\left(\theta\right),\tag{31}$$

<sup>&</sup>lt;sup>2</sup>Repeated indices do not imply summation in this work.

where the size of the stochastic matrix  $\mathbf{Q}^{\mathrm{T}}\mathbf{A}(\theta)\mathbf{Q} \in \mathbb{R}^{k \times k}$  is much smaller than the original SFEE (13), that is,  $k \ll n$ . Therefore, significant computational savings are achieved. Furthermore, we can solve Eq. (31) cheaply for a set of random sample realizations  $\left\{\theta^{(i)} \in \Theta\right\}_{i=1}^{n_{\mathrm{s}}}$  using MCS owing to the small size k. The total computational cost is still very low.

#### 3.2. Solution algorithm for SFEE of mass transport

In this section we extend the above iterative process to solve Eq. (19). To this end, the stochastic solution  $\mathbf{C}(t,\theta)$  is approximated using the following decoupled and greedy way

$$\mathbf{C}_{k}(t,\theta) = \sum_{i=1}^{k} \eta_{i}(\theta) g_{i}(t) \mathbf{h}_{i} = \mathbf{C}_{k-1}(t,\theta) + \Delta \mathbf{C}_{k}(t,\theta),$$
(32)

where  $\mathbf{C}_{k-1}(t,\theta) = \sum_{i=1}^{k-1} \eta_i(\theta) \, g_i(t) \, \mathbf{h}_i$  and  $\mathbf{C}_k(t,\theta)$  are the  $(k-1)^{\text{th}}$ - and  $k^{\text{th}}$  approximations of the stochastic solution  $\mathbf{C}(t,\theta)$ ,  $\{\eta_i(\theta)\}_{i=1}^k$  are a set of random variables,  $\{g_i(t)\}_{i=1}^k$  are a set of temporal functions,  $\{\mathbf{h}_i \in \mathbb{R}^n\}_{i=1}^k$  are a set of deterministic vectors, and  $\Delta \mathbf{C}_k(t,\theta) = \eta_k(\theta) \, g_k(t) \, \mathbf{h}_k$  is the  $k^{\text{th}}$  stochastic increment. Similarly, the set of triplets  $\{\eta_i(\theta), g_i(t), \mathbf{h}_i\}_{i=1}^k$  is not known a priori and needs to be solved one by one. Assuming that the approximation  $\mathbf{C}_{k-1}(t,\theta)$  has been known or given an initial value and substituting Eq. (32) into Eq. (19) we have

$$\mathcal{L}_{C}\left[\Delta \mathbf{C}_{k}\left(t,\theta\right)\right] = \mathbf{S}_{k}\left(t,\theta\right),\tag{33}$$

where the stochastic linear operator  $\mathcal{L}_C = \mathbf{M} \frac{\partial}{\partial t} + \mathbf{Z}(\theta) \in \mathbb{R}^{n \times n}$  and the stochastic right-side vector  $\mathbf{S}_k(t,\theta) = -\mathcal{L}_C[\mathbf{C}_{k-1}(t,\theta)] \in \mathbb{R}^n$ . Only the triplet  $\{\eta_k(\theta), g_k(t), \mathbf{h}_k\}$  is unknown, and they are solved using the following alternating iteration

$$\left[\iint_{\Theta\times\mathcal{T}}\eta_{k}^{2}\left(\theta\right)g_{k}\left(t\right)\mathcal{L}_{C}g_{k}\left(t\right)dtd\mathcal{P}\left(\theta\right)\right]\mathbf{h}_{k}=\iint_{\Theta\times\mathcal{T}}\eta_{k}\left(\theta\right)g_{k}\left(t\right)\mathbf{S}_{k}\left(t,\theta\right)dtd\mathcal{P}\left(\theta\right)\in\mathbb{R}^{n},\tag{34a}$$

$$\left[\int_{\Theta} \eta_{k}^{2}(\theta) \left(\mathbf{h}_{k}^{\mathrm{T}} \mathcal{L}_{C} \mathbf{h}_{k}\right) d\mathcal{P}(\theta)\right] g_{k}(t) = \int_{\Theta} \eta_{k}(\theta) \mathbf{h}_{k}^{\mathrm{T}} \mathbf{S}_{k}(t, \theta) d\mathcal{P}(\theta) \in \mathbb{R}, \tag{34b}$$

$$\left[\int_{\mathcal{T}} g_k(t) \left(\mathbf{h}_k^{\mathrm{T}} \mathcal{L}_C \mathbf{h}_k\right) g_k(t) \, \mathrm{d}t \right] \eta_k(\theta) = \int_{\mathcal{T}} \mathbf{h}_k^{\mathrm{T}} \mathbf{S}_k(t, \theta) g_k(t) \, \mathrm{d}t \in \mathbb{R}.$$
 (34c)

Given a known random variable  $\eta_k(\theta)$  and a known temporal function  $g_k(t)$  (or given their initial values), Eq. (34a) is a deterministic linear equation that is obtained by applying the stochastic Galerkin method [13, 14] and the time Galerkin method [23] to Eq. (33), which can be solved

efficiently and accurately using existing numerical solvers, even for very large problem sizes. With the known random variable  $\eta_k(\theta)$  and the known deterministic vector  $\mathbf{h}_k$  (obtained by Eq. (34a)), Eq. (34b) is a one-dimensional ordinary differential equation for  $g_k(t)$  that is obtained by applying the stochastic Galerkin method and the space Galerkin method to Eq. (33). This equation can also solved using existing solvers [37], even for very long-duration problems (i.e. a large temporal grid). With the known deterministic vector  $\mathbf{h}_k$  (obtained by Eq. (34a)) and the known temporal function  $g_k(t)$  (obtained by Eq. (34b)), Eq. (34c) is a one-dimensional stochastic algebraic equation that is obtained by applying the space and time Galerkin methods to Eq. (33), which can also be solved efficiently by the sample-based strategy used in Eq. (30), even for very high-dimensional stochastic problems. Also, during the iteration, we perform the orthonormalization  $\mathbf{h}_k^T \mathbf{h}_i = \delta_{ki}$ ,  $i \in \{1, k-1\}$  and the normalization  $\int_{\mathcal{T}} g_k^2(t) \, dt = 1$ . Moreover, we highlight that the implementations of Eq. (34) are inexpensive. Specifically, we have

$$\iint_{\Theta \times \mathcal{T}} \eta_k^2(\theta) g_k(t) \mathcal{L}_C g_k(t) dt d\mathcal{P}(\theta) = \mathbb{E}\left\{\eta_k^2(\theta)\right\} \int_{\mathcal{T}} \frac{\partial g_k(t)}{\partial t} g_k(t) dt + \mathbb{E}\left\{\eta_k^2(\theta) \mathbf{Z}(\theta)\right\}, \quad (35a)$$

$$\int_{\Theta} \eta_{k}^{2}(\theta) \left(\mathbf{h}_{k}^{\mathrm{T}} \mathcal{L}_{C} \mathbf{h}_{k}\right) d\mathcal{P}(\theta) = \mathbb{E}\left\{\eta_{k}^{2}(\theta)\right\} \left(\mathbf{h}_{k}^{\mathrm{T}} \mathbf{M} \mathbf{h}_{k}\right) \frac{\partial}{\partial t} + \mathbf{h}_{k}^{\mathrm{T}} \mathbb{E}\left\{\eta_{k}^{2}(\theta) \mathbf{Z}(\theta)\right\} \mathbf{h}_{k}, \quad (35b)$$

$$\int_{\mathcal{T}} g_k(t) \left( \mathbf{h}_k^{\mathrm{T}} \mathcal{L}_C \mathbf{h}_k \right) g_k(t) \, \mathrm{d}t = \left( \mathbf{h}_k^{\mathrm{T}} \mathbf{M} \mathbf{h}_k \right) \int_{\mathcal{T}} \frac{\partial g_k(t)}{\partial t} g_k(t) \, \mathrm{d}t + \mathbf{h}_k^{\mathrm{T}} \mathbf{Z}(\theta) \, \mathbf{h}_k, \tag{35c}$$

where  $\mathbb{E}\left\{\eta_k^2\left(\theta\right)\right\}$  and  $\mathbb{E}\left\{\eta_k^2\left(\theta\right)\mathbf{Z}\left(\theta\right)\right\}$  can be calculated cheaply for both low- and high-dimensional random inputs using their random sample realizations and are reused in both Eqs. (35a) and (35b),  $\int_{\mathcal{T}} \frac{\partial g_k(t)}{\partial t} g_k\left(t\right) dt$  is a scalar value even for long-duration problems, and  $\mathbf{h}_k^T \mathbf{M} \mathbf{h}_k$  and  $\mathbf{h}_k^T \mathbf{Z}\left(\theta\right) \mathbf{h}_k$  are deterministic and stochastic scalar values even for large-scale problems and are reused in both Eqs. (35b) and (35c). The right-side terms in Eq. (34) can be calculated cheaply in a similar way. To conclude, we highlight that the proposed iteration can handle large-scale, stochastically high-dimensional and long-duration problems very well.

Furthermore, similar to Eq. (31), we consider  $\mathbf{H} = [\mathbf{h}_1, \cdots, \mathbf{h}_k] \in \mathbb{R}^{n \times k}$  as a set of reduced bases and re-approximate the stochastic solution as  $\mathbf{C}(t, \theta) = \mathbf{H}\mathbf{G}(t, \theta)$ , where the time-dependent random vector  $\mathbf{G}(t, \theta) = [g_1(t, \theta), \cdots, g_k(t, \theta)]^T \in \mathbb{R}^k$  is introduced and  $g_i(t, \theta)$  are temporal-stochastic scalar-valued function. To improve the computational accuracy of the stochastic solu-

tion  $C(t, \theta)$ , the following time-dependent reduced-order SFEE is used to recalculate  $G(t, \theta)$ 

$$\left(\mathbf{H}^{\mathsf{T}}\mathcal{L}_{C}\mathbf{H}\right)\mathbf{G}\left(t,\theta\right) = \mathbf{0},\tag{36}$$

equivalently,

$$\mathbf{m}(\theta) \frac{\partial \mathbf{G}(t,\theta)}{\partial t} + \mathbf{z}(\theta) \mathbf{G}(t,\theta) = \mathbf{0}, \tag{37}$$

where the stochastic reduced-order matrices  $\mathbf{m}(\theta) = \mathbf{H}^{\mathrm{T}}\mathbf{M}(\theta)\mathbf{H} \in \mathbb{R}^{k \times k}$  and  $\mathbf{z}(\theta) = \mathbf{H}^{\mathrm{T}}\mathbf{Z}(\theta)\mathbf{H} \in \mathbb{R}^{k \times k}$  are much smaller. Therefore, we can use MCS to solve Eq. (37) cheaply for a set of sample realizations  $\left\{\theta^{(i)} \in \Theta\right\}_{i=1}^{n_{\mathrm{s}}}$ . The final stochastic solution of  $\mathbf{G}(t,\theta)$  is given by  $\mathbf{G}\left(\mathbf{t},\widehat{\boldsymbol{\theta}}\right) \in \mathbb{R}^{k \times n_{\mathrm{t}} \times n_{\mathrm{s}}}$ , where  $n_{\mathrm{t}}$  is the total number of time steps. This may involve a high storage requirement when  $n_{\mathrm{t}}$  and  $n_{\mathrm{s}}$  are large. To avoid this, we represent  $\mathbf{G}(t,\theta)$  as follows (this will be discussed later on)

$$\mathbf{G}(t,\theta) = \sum_{j=1}^{r_{\mathbf{G}}} \eta_j(\theta) \,\mathbf{G}_j(t), \qquad (38)$$

where the deterministic matrices  $\mathbf{G}_{j}(t) \in \mathbb{R}^{k \times n_{t}}$  and the random sample vectors  $\eta_{j}(\widehat{\boldsymbol{\theta}}) \in \mathbb{R}^{1 \times 1 \times n_{s}}$  (actually a vector-like tensor to match the dimension of  $\mathbf{G}(t,\theta)$ ). In this way, the storage requirement is reduced from  $\mathscr{O}(nn_{t}n_{s})$  for  $\mathbf{C}(t,\theta)$  in the original SFEE (19) to  $\mathscr{O}(kn_{t}n_{s})$  for  $\mathbf{G}(t,\theta)$  in the reduced-order SFEE (37), then to  $\mathscr{O}(r_{\mathbf{G}}(kn_{t}+n_{s}))$  for  $\mathbf{G}(t,\theta)$  in Eq. (38). More importantly, Eq. (38) provides a decoupled representation of stochastic and temporal components and incorporates all uncertainties into random sample vectors  $\left\{\eta_{j}(\widehat{\boldsymbol{\theta}})\right\}_{j=1}^{r_{\mathbf{G}}}$ . This is very convenient for subsequent uncertainty quantification analysis.

To further speed up the solution of Eq. (37), we propose a time parallel algorithm. Specifically, we use the Backward Euler time discretization to solve Eq. (37)

$$[\mathbf{m} + \mathbf{z}(\theta) \, \Delta t] \, \mathbf{G}_i(\theta) = \mathbf{m} \mathbf{G}_{i-1}(\theta), \tag{39}$$

where  $\mathbf{G}_{j}(\theta) = \mathbf{G}(t_{j}, \theta)$  is the solution at the time  $t_{j}$  and  $\Delta t$  is the time step. Eq. (39) can be further rewritten as

$$\mathbf{G}_{j}(\theta) = \left[\mathbf{m} + \mathbf{z}(\theta) \,\Delta t\right]^{-1} \mathbf{m} \mathbf{g}_{j-1}(\theta). \tag{40}$$

Following this, we perform the eigendecomposition  $[\mathbf{m} + \mathbf{z}(\theta) \Delta t]^{-1} \mathbf{m} = \mathbf{Q} \mathbf{A} \mathbf{Q}^{\mathrm{T}}$ , where  $\mathbf{Q}^{-1} = \mathbf{Q}^{\mathrm{T}} \in \mathbb{R}^{k \times k}$  is an orthogonal matrix consisting of all eigenvectors of the matrix  $[\mathbf{m} + \mathbf{z}(\theta) \Delta t]^{-1} \mathbf{m}$ 

and  $\mathbf{A} \in \mathbb{R}^{k \times k}$  is a diagonal matrix whose elements are the corresponding eigenvalues. Due to the small size of  $[\mathbf{m} + \mathbf{z}(\theta) \Delta t]^{-1} \mathbf{m}$ , the eigendecomposition is cheap enough, which is typically not applicable for the original SFEE (19) since the eigendecomposition of large-scale matrices is too expensive. Substituting the decomposition into Eq. (40) we can obtain the following time parallel solution

$$\mathbf{G}_{i}(\theta) = \mathbf{Q}\mathbf{A}^{j}\mathbf{Q}^{\mathsf{T}}\mathbf{G}_{0}(\theta), \tag{41}$$

where  $G_0(\theta)$  is given by initial conditions. Therefore, the solutions at different time steps are independent of each other and can be solved in parallel. Furthermore, it only requires calculating  $A^j$  at each time step, which is very cheap due to the diagonal property of the matrix A.

**Remark 1.** It is worth noting that the iteration in Eq. (34) may be unstable in the cases where the coefficient matrix  $\iint_{\Theta \times T} \eta_k^2(\theta) g_k(t) \mathcal{L}_C g_k(t) dt d\mathcal{P}(\theta) \in \mathbb{R}^{n \times n}$  in Eq. (34a) is ill-conditioned (may be caused by integration in the time domain), or the probability distributions of the scalar-valued coefficients  $\int_{\Theta} \eta_k^2(\theta) \left(\mathbf{h}_k^T \mathcal{L}_C \mathbf{h}_k\right) d\mathcal{P}(\theta)$  or  $\int_{\mathcal{T}} g_k(t) \left(\mathbf{h}_k^T \mathcal{L}_C \mathbf{h}_k\right) g_k(t) dt$  in Eqs. (34b) and (34c) contain the value zero (may be caused by integration in the time domain and the stochastic space). In these cases, we cannot obtain converged solutions. To overcome this, we can use the iteration proposed in our previous work [38], which is a bit more complex but sufficiently stable. Specifically, instead of the approximation  $\Delta \mathbf{C}_k(t,\theta) = \eta_k(\theta) g_k(t) \mathbf{h}_k$ , we use the following two approximations for the stochastic increment

$$\Delta \mathbf{C}_{k}(t,\theta) \approx \eta_{k}(\theta) \, \widetilde{\mathbf{h}}_{k}(t) \,, \tag{42a}$$

$$\approx \widetilde{g}_k(t,\theta)\,\mathbf{h}_k. \tag{42b}$$

where  $\widetilde{\mathbf{h}}_k(t)$  is the temporal-spatial coupled approximation of  $g_k(t)$  and  $\mathbf{h}_k$ , and  $\widetilde{g}_k(t,\theta)$  is the temporal-stochastic coupled approximation of  $g_k(t)$  and  $\eta_k(\theta)$ . The following alternating iteration is used to solve the triplet  $\{\eta_k(\theta), g_k(t), \mathbf{h}_k\}$ :

$$\mathbb{E}\left\{\eta_{k}^{2}\left(\theta\right)\mathcal{L}_{C}\right\}\widetilde{\mathbf{h}}_{k}\left(t\right)=\mathbb{E}\left\{\eta_{k}\left(\theta\right)\mathbf{S}_{k}\left(t,\theta\right)\right\},\qquad\widetilde{\mathbf{h}}_{k}\left(t\right)=\mathbf{h}_{k}g_{k}\left(\mathbf{t}\right)\in\mathbb{R}^{n\times n_{t}},\ g_{k}\left(\mathbf{t}\right)\in\mathbb{R}^{1\times n_{t}},$$
(43a)

$$\left(\mathbf{h}_{k}^{\mathrm{T}}\mathcal{L}_{C}\mathbf{h}_{k}\right)\widetilde{g}_{k}\left(t,\theta\right) = \mathbf{h}_{k}^{\mathrm{T}}\mathbf{S}_{k}\left(t,\theta\right), \qquad \widetilde{g}_{k}\left(t,\widehat{\boldsymbol{\theta}}\right) = \eta_{k}\left(\widehat{\boldsymbol{\theta}}\right)g_{k}\left(\mathbf{t}\right) \in \mathbb{R}^{n_{\mathrm{s}} \times n_{\mathrm{t}}}, \quad \eta_{k}\left(\widehat{\boldsymbol{\theta}}\right) \in \mathbb{R}^{n_{\mathrm{s}}}. \quad (43b)$$

For a known random variable  $\eta_k(\theta)$ , considering the approximation Eq. (42a) and applying the stochastic Galerkin method to Eq. (33), we obtain Eq. (43a), which is a linear time-dependent

equation and can be solved efficiently using existing solvers. To achieve the temporal-spatial decoupled approximation of  $g_k(t)$  and  $\mathbf{h}_k$ , the rank-1 singular value decomposition (SVD) is further used in Eq. (43a). With the obtained vector  $\mathbf{h}_k$ , considering the approximation Eq. (42b) and applying the space Galerkin method to Eq. (33) we obtain Eq. (43b), which is a one-dimensional stochastic ordinary differential equation and can be solved cheaply using MCS. To achieve the temporal-stochastic decoupled approximation of  $g_k(t)$  and  $\eta_k(\theta)$ , the randomized rank-1 SVD is further used in Eq. (43b). In this way, the iteration in Eq. (43) is stable enough. The effectiveness and more numerical details of this method can be found in [38].

#### 3.3. High-dimensional random inputs

In this section we highlight the effectiveness of the proposed method handling high-dimensional random inputs without any modification, although this has already been hinted at above. Specifically, we explicitly introduce high-dimensional random inputs by setting large values  $r_K$  in Eq. (11) and  $r_Z$  in Eq. (22). On the basis of this, the calculations involving high-dimensional random inputs, including the expectations  $\mathbb{E}\left\{\lambda_k^2\left(\theta\right)\mathbf{A}\left(\theta\right)\right\}$  in Eq. (26) and  $\mathbb{E}\left\{\eta_k^2\left(\theta\right)\mathbf{Z}\left(\theta\right)\right\}$  in Eq. (35), as well as the vector-stochastic matrix multiplication  $\mathbf{d}_k^T\mathbf{A}\left(\theta\right)\mathbf{d}_k$  in Eq. (29) and  $\mathbf{h}_k^T\mathbf{Z}\left(\theta\right)\mathbf{h}_k$  in Eq. (35), are given by

$$\mathbb{E}\left\{\lambda_{k}^{2}\left(\theta\right)\mathbf{A}\left(\theta\right)\right\} = \sum_{j=0}^{r_{K}} \mathbb{E}\left\{\lambda_{k}^{2}\left(\theta\right)\xi_{j}\left(\theta\right)\right\}\mathbf{A}_{j}, \qquad \mathbb{E}\left\{\eta_{k}^{2}\left(\theta\right)\mathbf{Z}\left(\theta\right)\right\} = \sum_{j=0}^{r_{Z}} \mathbb{E}\left\{\lambda_{k}^{2}\left(\theta\right)\chi_{j}\left(\theta\right)\right\}\mathbf{Z}_{j}, \quad (44a)$$

$$\mathbf{d}_{k}^{\mathrm{T}}\mathbf{A}\left(\theta\right)\mathbf{d}_{k} = \sum_{j=0}^{r_{K}} \left(\mathbf{d}_{k}^{\mathrm{T}}\mathbf{A}_{j}\mathbf{d}_{k}\right)\xi_{j}\left(\theta\right), \qquad \mathbf{h}_{k}^{\mathrm{T}}\mathbf{Z}\left(\theta\right)\mathbf{h}_{k} = \sum_{j=0}^{r_{\mathbf{Z}}} \left(\mathbf{d}_{k}^{\mathrm{T}}\mathbf{Z}_{j}\mathbf{d}_{k}\right)\chi_{j}\left(\theta\right). \tag{44b}$$

It can be seen that Eq. (44a) only involves the expectations of random variables and Eq. (44b) only involves vector-deterministic matrix multiplication. Both equations are cheap enough, even for very high-dimensional random inputs. More importantly, their computational effort is insensitive to the stochastic dimension and proportionally increases as the stochastic dimension increases. In this sense, the proposed method successfully avoids the curse of dimensionality occurring in high-dimensional stochastic spaces.

#### 3.4. Efficient propagation of stochastic quantities

In this section we address the issue of efficient propagation of stochastic quantities. To generate Eq. (19), we need to calculate the stochastic velocity  $v(\theta)$  and the stochastic diffusion-dispersion coefficient  $D(\theta)$  using the stochastic pressure obtained by Eq. (13), and then propagate them into Eq. (19). In fact, this is not trivial for many cases. Specifically, the stochastic velocity matrix (including two spatial directions) calculated through Eq. (2) is given by

$$\mathbf{v}(\theta) = \frac{\mathbf{q}(\theta)}{\phi} = -\sum_{j=0}^{r_K} \xi_j(\theta) \left( \sum_{i=1}^k \lambda_i(\theta) \left[ \nabla_x \mathbf{d}_i, \nabla_z \mathbf{d}_i \right]^{\mathrm{T}} - \rho \mathbf{g} \right) \mathbf{K}_{\phi\mu, j} \in \mathbb{R}^{2 \times n}, \tag{45}$$

where  $\mathbf{K}_{\phi\mu,j}$  is a diagonal matrix whose diagonal elements are the evaluation of  $\frac{K_j}{\phi\mu}$  at each spatial discretized node ( $K_j$  is given in Eq. (11)). Rewriting  $\mathbf{v}(\theta)$  as a vector form we have

$$\widetilde{\mathbf{v}}(\theta) = -\sum_{j=0}^{r_K} \sum_{i=1}^{k} \xi_j(\theta) \lambda_i(\theta) \underbrace{\begin{bmatrix} \mathbf{K}_{\phi\mu,j} (\nabla_x \mathbf{d}_i - \rho g_x \mathbb{1}_{n \times 1}) \\ \mathbf{K}_{\phi\mu,j} (\nabla_y \mathbf{d}_i - \rho g_y \mathbb{1}_{n \times 1}) \end{bmatrix}}_{=-\mathbf{f}_{ii} \in \mathbb{R}^{2n}} = \sum_{j=0}^{r_K} \sum_{i=1}^{k} \xi_j(\theta) \lambda_i(\theta) \mathbf{f}_{ji} \in \mathbb{R}^{2n}, \quad (46)$$

where  $\mathbb{1}_{n\times 1} \in \mathbb{R}^n$  is the all-ones vector. If  $k \cdot r_K$  is a large number, we have to calculate numerous terms  $\mathbf{f}_{ji}$ , which further leads to the need of a large amount of matrix assembly and storage for  $\{\mathbf{Z}_i\}_{i=1}^{r_K k}$  in Eq. (22). Therefore, the solution and storage of Eq. (22) will be quite expensive. A similar issue also occurs with the stochastic diffusion-dispersion coefficient  $\mathbf{D}(\theta)$ .

To address the above issue, we consider the following low-rank decoupled approximation

$$\widetilde{\mathbf{v}}(\theta) = \sum_{l=1}^{r_{\nu}} \chi_{\nu,l}(\theta) \, \mathbf{v}_l, \tag{47}$$

where  $\chi_{v,l}(\theta) \in \mathbb{R}$  and  $\mathbf{v}_l \in \mathbb{R}^{2n}$  are unknown random variables and deterministic vectors, respectively. A greedy iteration is used to solve each pair

$$\chi_{\nu,r}(\theta) \mathbf{v}_r = \widetilde{\mathbf{v}}(\theta) - \sum_{l=1}^{r-1} \chi_{\nu,l}(\theta) \mathbf{v}_l.$$
 (48)

Here assuming that  $\{\chi_{\nu,l}(\theta), \mathbf{v}_l\}_{l=1}^{r-1}$  have been known, we only need to solve the pair  $\{\chi_{\nu,r}(\theta), \mathbf{v}_r\}$ . The following alternating iteration is used for this purpose

$$\mathbb{E}\left\{\chi_{\nu,r}^{2}(\theta)\right\}\mathbf{v}_{r} = \mathbb{E}\left\{\chi_{\nu,r}(\theta)\left[\widetilde{\mathbf{v}}(\theta) - \sum_{l=1}^{r-1}\chi_{\nu,l}(\theta)\,\mathbf{v}_{l}\right]\right\} \in \mathbb{R}^{2n},\tag{49a}$$

$$\left(\mathbf{v}_{r}^{\mathrm{T}}\mathbf{v}_{r}\right)\chi_{\mathbf{v},r}\left(\theta\right) = \mathbf{v}_{r}^{\mathrm{T}}\left[\widetilde{\mathbf{v}}\left(\theta\right) - \sum_{l=1}^{r-1}\chi_{\mathbf{v},l}\left(\theta\right)\mathbf{v}_{l}\right] \in \mathbb{R}.$$
(49b)

Given a known random variable  $\chi_{v,r}(\theta)$ , Eq. (49a) is obtained by applying the stochastic Galerkin method to Eq. (48), and with the known deterministic vector  $\mathbf{v}_r$  obtained by Eq. (48), Eq. (49b) is obtained by applying the Galerkin method to Eq. (48). We still perform the orthonormalization  $\mathbf{v}_r^T\mathbf{v}_i = \delta_{ri}$ ,  $i \in \{1, r-1\}$  during the iteration. Considering Eq. (46) and the orthonormalization, Eq. (49) is further rewritten as

$$\mathbf{v}_{r} = \frac{1}{\mathbb{E}\left\{\chi_{\mathbf{v},r}^{2}(\theta)\right\}} \left[ \sum_{j=0}^{r_{K}} \sum_{i=1}^{k} \mathbb{E}\left\{\chi_{\mathbf{v},r}(\theta) \,\xi_{j}(\theta) \,\lambda_{i}(\theta)\right\} \mathbf{f}_{ji} - \sum_{l=1}^{r-1} \mathbb{E}\left\{\chi_{\mathbf{v},r}(\theta) \,\chi_{\mathbf{v},l}(\theta)\right\} \mathbf{v}_{l} \right], \tag{50a}$$

$$\chi_{\mathbf{v},r}(\theta) = \sum_{j=0}^{r_K} \sum_{i=1}^k \xi_j(\theta) \,\lambda_i(\theta) \left( \mathbf{v}_r^{\mathrm{T}} \mathbf{f}_{ji} \right), \tag{50b}$$

where  $\mathbb{E}\left\{\chi_{v,r}(\theta)\xi_j(\theta)\lambda_i(\theta)\right\}$  and  $\mathbb{E}\left\{\chi_{v,r}(\theta)\chi_{v,l}(\theta)\right\}$  are calculated cheaply by using sample realizations of these random variables, and  $\mathbf{v}_r^T\mathbf{f}_{ji}$  only involves vector-vector multiplication. Therefore, Eq. (50) has very low computational effort. Furthermore, by using a similar way, we can achieve other decoupled representations in Eqs. (21) and (38).

#### 4. Algorithm implementations

The proposed algorithm for solving the SFEE of Darcy flow is summarized in Algorithm 1. It consists of double loops and a recalculation process. From step 2 to step 13, the outer loop is used to solve all potential pairs  $\{\lambda_i(\theta), \mathbf{d}_i\}_{i=1}^k$ , and from step 5 to step 10, the inner loop is used to solve each pair  $\{\lambda_k(\theta), \mathbf{d}_k\}$ . For the inner loop, a nonzero vector of size  $n_s$  is given in step 4 as the initialization of the random variable  $\lambda_k(\theta)$ . The intermediate vector  $\mathbf{d}_k^{(j)}$  during iteration is orthonormalized in step 7 using the Gram–Schmidt method. Following the outer loop, a recalculation process is performed to update the random variable vector  $\mathbf{\Lambda}(\theta)$  for a set of random sample realizations. Furthermore, there are two iterative indicators in step 9 and step 12 used to check the convergence of the inner and outer loops, respectively. The indicator  $\epsilon_{\mathbf{d},j}$  in step 9 measures the difference between the vectors  $\mathbf{d}_k^{(j)}$  and  $\mathbf{d}_k^{(j-1)}$ , where  $\|\cdot\|_2$  is the  $L_2$  norm. The indicator  $\epsilon_{p,k}$  in step

# Algorithm 1 Algorithm for solving the SFEE of Darcy flow

- 1: Assemble the stochastic matrix  $\mathbf{A}(\theta) \in \mathbb{R}^{n \times n}$  and the stochastic vector  $\mathbf{B}(\theta) \in \mathbb{R}^n$  in Eq. (13),  $k \leftarrow 1$
- 2: while  $\epsilon_{p,k} > \epsilon_p \operatorname{do}$
- 3: Update the right-side vector  $\mathbf{B}_{k}(\theta) = \mathbf{B}(\theta) \mathbf{A}(\theta) \mathbf{p}_{k-1}(\theta) \in \mathbb{R}^{n}$
- 4: Initialize the random sample vector  $\lambda_k^{(0)}(\widehat{\boldsymbol{\theta}}) \in \mathbb{R}^{n_{\rm s}}$
- 5: **while**  $\epsilon_{\mathbf{d},j} > \epsilon_{\mathbf{d}}$  **do**
- 6: Solve the deterministic vector  $\mathbf{d}_{k}^{(j)} \in \mathbb{R}^{n}$  using Eq. (26)
- 7: Orthonormalize the vector  $\mathbf{d}_k^{(j)}$  using Eq. (27)
- 8: Solve the sample vector  $\lambda_k^{(j)}(\widehat{\boldsymbol{\theta}}) \in \mathbb{R}^{n_s}$  using Eq. (30)
- 9: Calculate the iterative error  $\epsilon_{\mathbf{d},j} = \left\| \mathbf{d}_k^{(j)} \mathbf{d}_k^{(j-1)} \right\|_2^2, j \leftarrow j + 1$
- 10: **end**
- 11: Update the deterministic matrix  $\mathbf{D} = [\mathbf{D}, \mathbf{d}_k] \in \mathbb{R}^{n \times k}$
- 12: Calculate the iterative error  $\epsilon_{p,k}$ ,  $k \leftarrow k+1$
- 13: **end**
- 14: Recalculate the sample realizations of  $\Lambda(\theta)$  using Eq. (31)

12 is given by

$$\epsilon_{p,k} = \frac{\mathbb{E}\left\{ \|\mathbf{p}_{k}\left(\theta\right) - \mathbf{p}_{k-1}\left(\theta\right)\|_{2}^{2} \right\}}{\mathbb{E}\left\{ \|\mathbf{p}_{k}\left(\theta\right)\|_{2}^{2} \right\}} = \frac{\mathbb{E}\left\{ \lambda_{k}^{2}\left(\theta\right) \right\} \mathbf{d}_{k}^{\mathrm{T}} \mathbf{d}_{k}}{\sum_{i,i=1}^{k} \mathbb{E}\left\{ \lambda_{i}\left(\theta\right) \lambda_{j}\left(\theta\right) \right\} \mathbf{d}_{i}^{\mathrm{T}} \mathbf{d}_{j}} = \frac{\mathbb{E}\left\{ \lambda_{k}^{2}\left(\theta\right) \right\}}{\sum_{i=1}^{k} \mathbb{E}\left\{ \lambda_{i}^{2}\left(\theta\right) \right\}},$$
(51)

which measures the contribution of the  $k^{\text{th}}$  pair  $\{\lambda_k(\theta), \mathbf{d}_k\}$  to the stochastic solution  $\mathbf{p}_k(\theta)$ . In practice,  $\epsilon_{p,k}$  does not keep decreasing for some cases since the random variables  $\{\lambda_i(\theta)\}_{i=1}^k$  are solved in a greedy way. To improve this, an eigendecomposition is performed:  $\mathbb{E}\left\{\mathbf{\Lambda}(\theta)\mathbf{\Lambda}(\theta)^T\right\} = \mathbf{Q}\Psi\mathbf{Q}^T$ , where  $\Psi$  is a diagonal matrix and  $\mathbf{Q} \in \mathbb{R}^{k \times k}$  is an orthonormal matrix satisfying  $\mathbf{Q}\mathbf{Q}^T = \mathbf{I}_k$ . The stochastic solution is re-represented as  $\mathbf{p}_k(\theta) = \mathbf{D}\mathbf{Q}\mathbf{Q}^T\mathbf{\Lambda}(\theta)$ , which does not improve the computational accuracy but only provides a new representation. Substituting it into Eq. (51) and introducing an equivalent vector  $\mathbf{Q}^T\mathbf{\Lambda}(\theta) = \left[\widetilde{\lambda}_1(\theta), \cdots, \widetilde{\lambda}_k(\theta)\right]^T \in \mathbb{R}^k$ , we have

$$\epsilon_{p,k} = \frac{\mathbb{E}\left\{\widetilde{\lambda}_{k}^{2}(\theta)\right\}}{\sum_{i=1}^{k} \mathbb{E}\left\{\widetilde{\lambda}_{i}^{2}(\theta)\right\}} = \frac{\psi_{k}}{\operatorname{Tr}(\boldsymbol{\Psi})},$$

$$23$$
(52)

# Algorithm 2 Algorithm for solving the SFEE of mass transport

```
1: Assemble the stochastic matrices \mathbf{M} \in \mathbb{R}^{n \times n} and \mathbf{Z}(\theta) \in \mathbb{R}^{n \times n} in Eq. (19), k \leftarrow 1
 2: while \epsilon_{C,k} > \epsilon_C do
             Update the right-side vector \mathbf{S}_k(t, \theta) \in \mathbb{R}^n
 3:
            Initialize the random sample vector \eta_k^{(0)}(\widehat{\boldsymbol{\theta}}) \in \mathbb{R}^{n_s}
 4:
 5:
             while \epsilon_{\mathbf{h},j} > \epsilon_{\mathbf{h}} do
                   Solve the deterministic vector \mathbf{h}_{k}^{(j)} \in \mathbb{R}^{n} using Eq. (34a)
 6:
                   Orthogonalize the vector \mathbf{h}_{l}^{(j)} using Eq. (27)-like process
 7:
                   Solve the temporal function g_k^{(j)}(\mathbf{t}) \in \mathbb{R}^{1 \times n_t} using Eq. (34b)
 8:
                   Solve the sample vector \eta_k^{(j)}(\widehat{\boldsymbol{\theta}}) \in \mathbb{R}^{n_s} using Eq. (34c)
 9:
                   Calculate the iterative error \epsilon_{\mathbf{h},j} = \left\| \mathbf{h}_{k}^{(j)} - \mathbf{h}_{k}^{(j-1)} \right\|_{2}^{2}, j \leftarrow j + 1
10:
            end
11:
             Update the deterministic matrix \mathbf{H} = [\mathbf{H}, \mathbf{h}_k] \in \mathbb{R}^{n \times k}
12:
            Calculate the iterative error \epsilon_{C,k}, k \leftarrow k + 1
13:
14: end
15: Recalculate the sample realizations of G(t, \theta) using Eq. (41)
16: Generate the decoupled representation (38) using Algorithm 3
```

where  $\text{Tr}(\cdot)$  is the trace operator and  $\psi_k$  is the  $k^{\text{th}}$  diagonal element of the matrix  $\Psi$ . In this way, the iterative indicator  $\epsilon_{p,k}$  keeps decreasing as the item k increases.

Similar to Algorithm 1, the proposed method for solving the SFEE of mass transport is summarized in Algorithm 2, where all notations are the same as in Algorithm 1. Compared to Algorithm 1, an additional step is used in step 8 to solve the temporal component, and following the recalculation step 15, an additional step in step 16 is introduced to generate a decoupled representation of the temporal-stochastic solution. In addition, if the inner iteration from step 5 to step 11 is unstable, it needs to be replaced using the method given in Remark 1. According to our numerical tests, the problem that this article focuses on is sufficiently stable.

The proposed method for propagating stochastic quantities is also summarized in Algorithm 3, which has similar structure to Algorithm 1 and Algorithm 2. However, this algorithm is much

## Algorithm 3 Algorithm for propagating stochastic quantities

- 1: Giving a stochastic quantity, e.g.,  $\widetilde{\mathbf{v}}(\theta)$  in Eq. (46) and  $\mathbf{G}(t,\theta)$  in Eq. (37),  $k \leftarrow 1$
- 2: while  $\epsilon_{q,k} > \epsilon_q$  do
- 3: Initialize the random sample vector  $\chi_{v,k}^{(0)}(\widehat{\boldsymbol{\theta}}) \in \mathbb{R}^{n_{\rm s}}$
- 4: **while**  $\epsilon_{\mathbf{v},j} > \epsilon_{\mathbf{v}} \mathbf{do}$
- 5: Solve the deterministic vector  $\mathbf{v}_{k}^{(j)} \in \mathbb{R}^{n}$  using Eq. (50a)
- 6: Orthogonalize the vector  $\mathbf{v}_{k}^{(j)}$  using Eq. (27)-like process
- 7: Solve the sample vector  $\chi_{v,k}^{(j)}(\widehat{\boldsymbol{\theta}}) \in \mathbb{R}^{n_s}$  using Eq. (50b)
- 8: Calculate the iterative error  $\epsilon_{\mathbf{v},j} = \left\| \mathbf{v}_k^{(j)} \mathbf{v}_k^{(j-1)} \right\|_2^2, j \leftarrow j + 1$
- 9: **end**
- 10: Store the vector:  $[\mathbf{v}_1, \dots, \mathbf{v}_{k-1}, \mathbf{v}_k] \in \mathbb{R}^{n \times k}$
- 11: Store the sample vector:  $\left[\chi_{\nu,1}\left(\widehat{\boldsymbol{\theta}}\right), \cdots, \chi_{\nu,k-1}\left(\widehat{\boldsymbol{\theta}}\right), \chi_{\nu,k}\left(\widehat{\boldsymbol{\theta}}\right)\right] \in \mathbb{R}^{n_s \times k}$
- 12: Calculate the iterative error  $\epsilon_{q,k}$ ,  $k \leftarrow k + 1$
- 13: **end**

more efficient since it does not require solving systems of linear equations.

#### 5. Numerical results

In this section we verify the proposed framework using a numerical example. For all algorithms, the sample size of the iterative processes is  $n_s = 1 \cdot 10^4$ , and the convergence criteria of inner iterations are set to  $\varepsilon_d = \varepsilon_h = \varepsilon_v = 1 \cdot 10^{-3}$ . Reference solutions are obtained by  $1 \cdot 10^4$  standard Monte Carlo simulations, which is sufficient to achieve converged stochastic solutions according to numerical tests. Furthermore, to eliminate the influence caused by the sampling process itself, the same  $1 \cdot 10^4$  random sample realizations are used in the proposed scheme. All tests are performed on a desktop computer (sixteen cores, Intel Core i7, 2.5 GHz), but only a single core is used for the numerical implementation.

#### 5.1. Model inputs

As mentioned in Section 2.1, a 2D model is created considering different material groups surrounding a reference containment-providing rock zone (r-CRZ) in the context of an m-mCRZ

Table 1: Model parameters

Quantity	Unit	Value
Porosity $\phi$ :	_	
MG* I&II		0.01 [39]
MG III		0.36 [40]
Permeability $K(\mathbf{x}, \theta)$	$m^2$	[39]
MGI		$K_0 = 5 \cdot 10^{-16}, \sigma_K = 0.2 K_0$
MG II&III		$[1 \cdot 10^{-20}, 1 \cdot 10^{-18}]$
Pore diffusion coefficient $D_{ m f}$	$m^2  s^{-1}$	
MG I&II		$1 \cdot 10^{-10}  [41]$
MGI		$5 \cdot 10^{-10}$
Bulk density of the porous medium $\rho_b$	${\rm kg}{\rm m}^{-3}$	
MG I&II		2650 [41]
MG III		2700 [40]
Liquid viscosity $\mu$	$Pa \cdot s$	0.001
Dispersivity $\alpha_{\rm L}, \alpha_{\rm T}$	m	20, 5 [41]
$^{129}$ I sorption coefficient $k_{\rm d}$	$m^3 kg^{-1}$	0 [41]
$^{129}$ I half life $t_{1/2}$	a	$15.7 \cdot 10^6  [41]$

repository concept in crystalline rock. The model parameters are listed in Table 1, where most parameter values are sourced from the literature. Homogeneous material properties are assigned for material groups representing the emplacement zone (MG III) and bentonite buffer (MG II). Furthermore, a two-layer diffusion system is considered, with different diffusion coefficients assigned for bentonite buffer and crystalline rock. In accordance with the German Site Selection Act for high-level waste repositories (StandAG)[1], the minimum permeability requirement for the barrier system is less than  $1 \cdot 10^{-17}$  m<sup>2</sup>. Consequently, uniformly distributed random variables within the range of  $\left[10^{-20},\ 10^{-18}\right]$  m<sup>2</sup> are applied for the permeability of the intact rock and the

bentonite buffer layers. Furthermore, permeability values in MG II and MG III are assumed to be independent. To represent the impact of fractures and fracture networks on hydraulic properties, the permeability of the fractured rock mass (MG I) is modeled as a random field with the mean value  $K_0 = 5 \cdot 10^{-16} \,\mathrm{m}^2$  and the standard deviation  $\sigma_K = 1 \cdot 10^{-16} \,\mathrm{m}^2$  (i.e. a COV of 0.2). Due to its long half-life and minimal sorption effect on crystalline rock, the radionuclide <sup>129</sup>I is expected to have the highest transport potential. Therefore, this simulation focuses primarily on studying the transport behavior of <sup>129</sup>I, but other radionuclides can also be easily simulated using the proposed framework. <sup>129</sup>I is conservatively considered to be homogeneously distributed initially within the emplacement zone (MG III) (Fig. 1b). The value of the initial concentration (Table 2) is defined based on the total inventory suggested by [42]. In all other material groups, the initial concentration of <sup>129</sup>I is set to zero. The starting time for the modeling is defined as the time of canister failure, marking the onset of radionuclide release and subsequent transport. As the boundary condition for groundwater flow, a hydraulic gradient in the horizontal direction is given by defining differing Dirichlet boundary conditions for pressure at the left and right boundaries (Fig. 1b). Further initial and boundary conditions are given in Table 2.

The finite element mesh is shown in Fig. 2. The spatial discretization generates a total of 30 295 nodes and 60 304 linear triangle elements, where a gradient mesh is used, with a finer mesh for the inside part. For the random permeability field in Eq. (11) of the fractured rock mass, the correlation lengths are  $l_x = l_y = 20$  m, and the truncation term is r = 72 to achieve a truncation error of  $\chi_r / \sum_{i=1}^{r_K} \chi_i < 1 \cdot 10^{-2}$ . Therefore, this problem involves a total of 74 random variables (i.e., 72 Gaussian random variables and two uniform random variables), leading to the subsequent high-dimensional stochastic analysis. Three sample realizations of the random field  $K(x, z, \theta^{(*)})$  are shown in Fig. 3. It can be seen that these sample realizations involve strong spatial inhomogeneity. It is noted that random samples  $\theta^{(i)}$  with  $\min_{x,z} K(x,z,\theta^{(i)}) \le 1 \cdot 10^{-25}$  are discarded to ensure that all realizations are physically meaningful. Since the discarded sample interval has a very low probability of occurring, this truncation will actually cause minimal impact on the distribution change. It is worth noting that even if the distributions of random inputs were changed to non-Gaussian, the proposed method would still work without any modification due to its use of the sample-based strategy.

Table 2: Initial and boundary conditions (ICs/BCs)

Quantity	Unit	Value
Flow equation:		
Boundary conditions*		. (7)
zero-flux BC at $\Gamma_t$ and $\Gamma_b$ : $\mathbf{q} \cdot \mathbf{n} = 0$		
Dirichlet BC at $\Gamma_1$ : $p_1$	Pa	$1.82\cdot 10^5$
Dirichlet BC $\Gamma_r$ : $p_r$	Pa	$1.00\cdot10^5$
Solute transport:		
Initial conditions		
$C_{I-129}^0$ in MGIII	${\rm g}{\rm m}^{-3}$	0.186
$C_{I-129}^0$ in MGI and MGII	$g m^{-3}$	0
Boundary conditions		
zero-flux BC at $\Gamma_1$ and $\Gamma_r$ : $\nabla C \cdot \mathbf{n} = 0$		
Dirichlet BC at $\Gamma_{\rm t}$ and $\Gamma_{\rm b}$ : $C_{\rm I-129}$	$\mathrm{g}\mathrm{m}^{-3}$	0
* The boundaries $\Gamma_t$ , $\Gamma_b$ , $\Gamma_r$ , $\Gamma_l$ are illustrated in $\Gamma_t$	Fig. 1b	

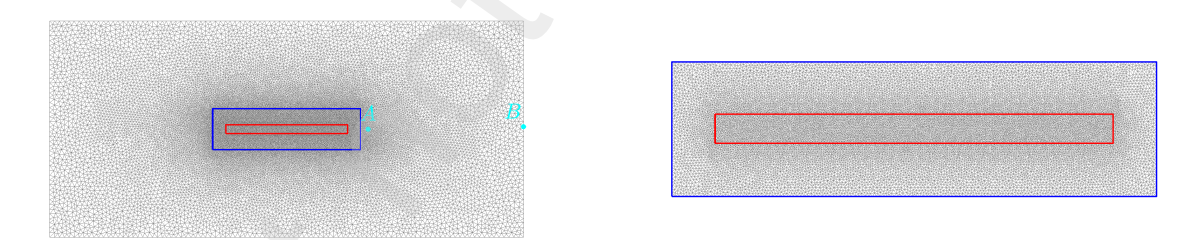


Figure 2: Finite element mesh: Mesh of the entire domain and location of two reference points A and B (left); zoomed in mesh of the inner part (right).

## 5.2. Results of stochastic Darcy flow

By using Algorithm 1 to solve Eq. (13), the stopping criterion in step 2 is set to  $\varepsilon_p = 1 \cdot 10^{-10}$ , and the corresponding iterative errors of different retained items are shown in Fig. 4. It can be seen that 35 retained items are sufficient to achieve the specified accuracy, which demonstrates the good convergence of the proposed method in solving the stochastic Darcy flow. Moreover, the

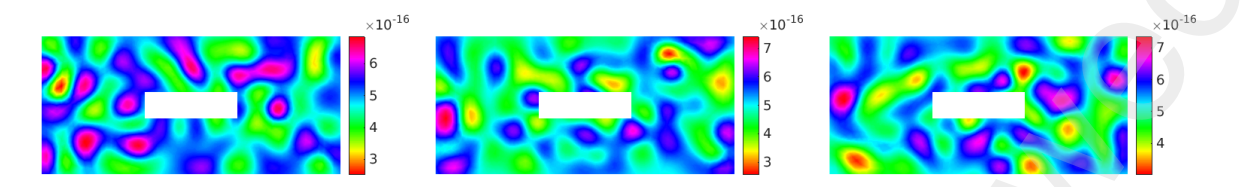


Figure 3: Three exemplary sample realizations of the permeability random field  $K(x, z, \theta^{(*)})$ .

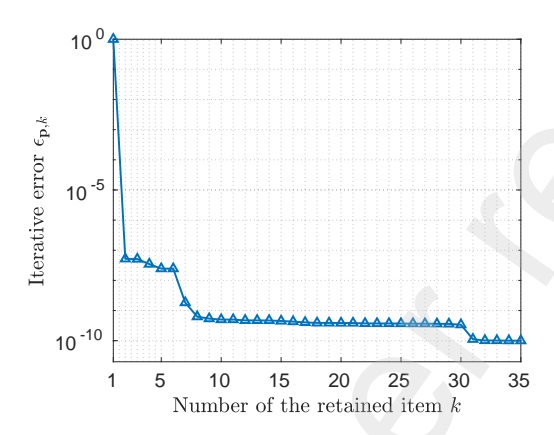


Figure 4: Iterative errors of different retained items.

iterative error keeps decreasing, which is consistent with the discussion of Eq. (52). Six solution components of the stochastic pressure field are shown in Fig. 5, including the deterministic vectors and the probability density functions (PDFs) of the corresponding random variable coefficients. Among the selected modes, we see a clear dominance of the linear component of the pressure field,  $\mathbf{d}_1$ , in accordance with the boundary conditions (primary solution). The remaining modes constitute roughly zero-mean fluctuations around this primary pressure field. Different modes of spatial vectors can be captured well and used to approximate the stochastic pressure accurately.

In terms of computational accuracy, we focus on the PDF of the stochastic pressure at the interior center point. PDFs obtained using a different number of retained items  $k = \{10, 20, 35\}$  are shown in Fig. 6a and their absolute errors relative to the MCS reference PDF can be seen from Fig. 6b. Even 10 retained items can provide a good approximation for the stochastic pressure. It is important to note that as the number of retained items increases, a decrease of the approximation error is observed. Therefore, if a more accurate stochastic solution is needed, more items should be retained. Furthermore, we highlight that even for each sample realization of random inputs,

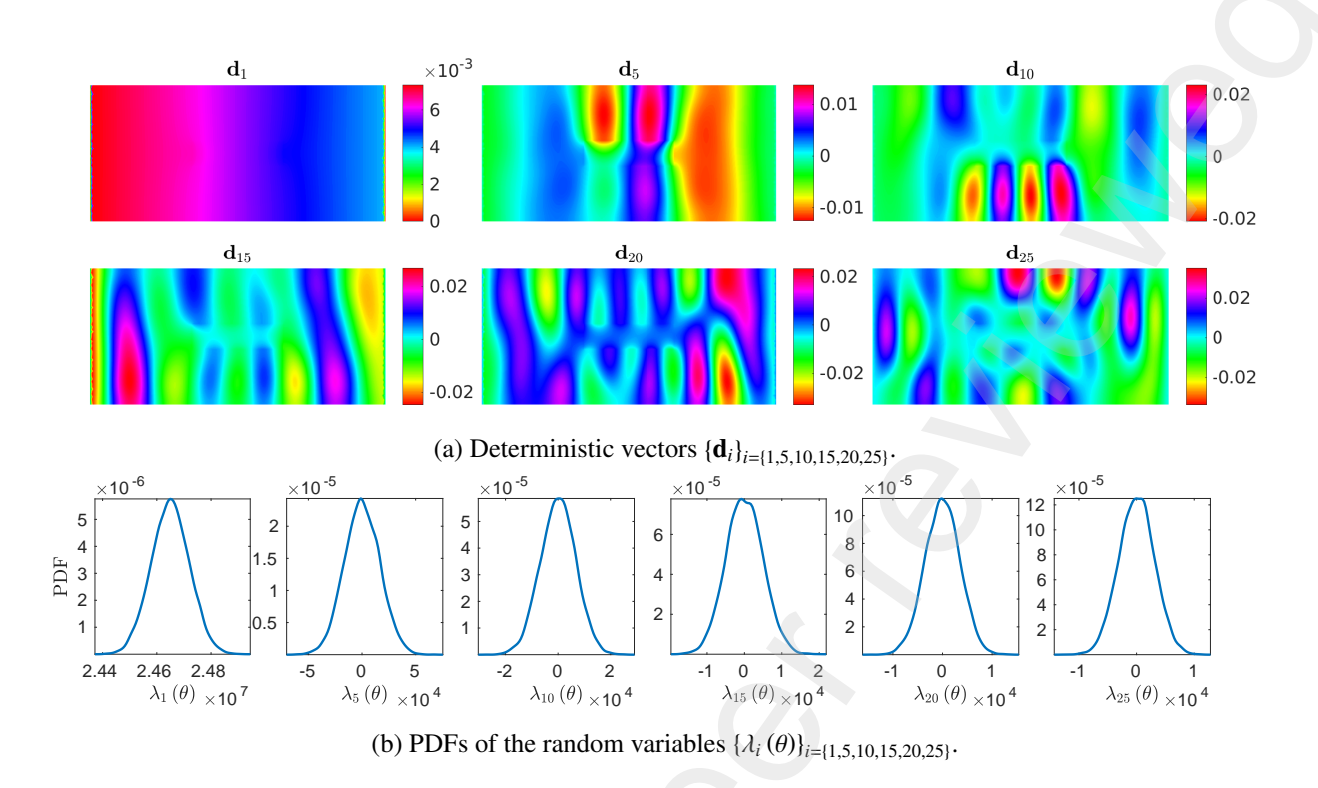


Figure 5: Solution components of the stochastic pressure field: Selected deterministic vectors (top) and PDFs of the corresponding random variable coefficients (bottom).

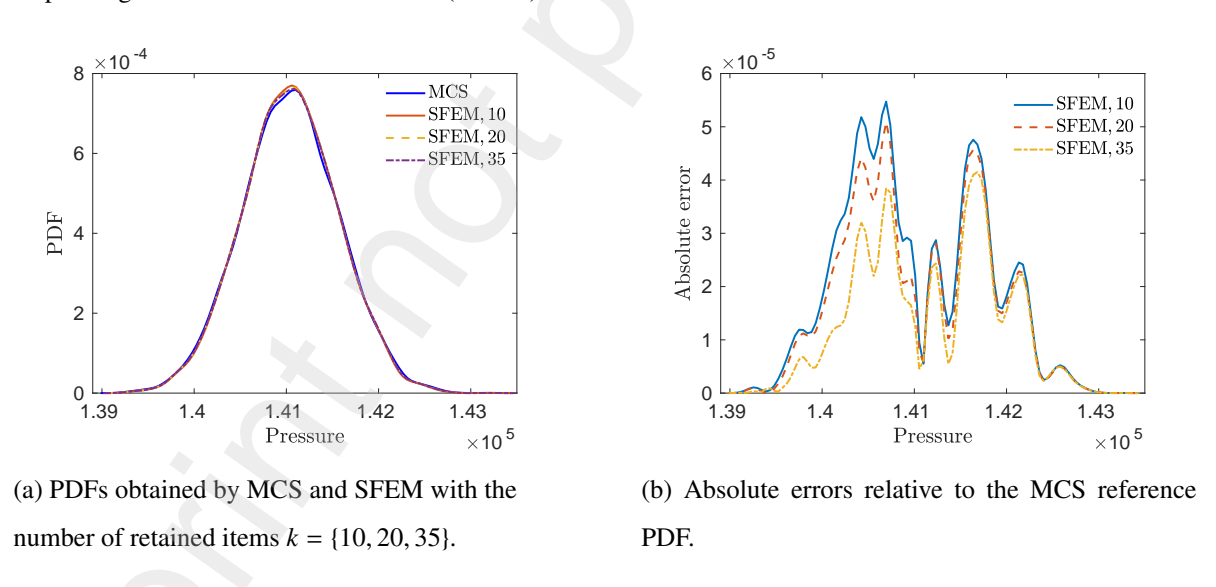


Figure 6: PDFs of the stochastic pressure (Pa) at the domain's mid point.

the proposed method is still accurate enough. For a given random sample realization, the sample realizations of stochastic pressure obtained by the proposed method and MCS, and their relative

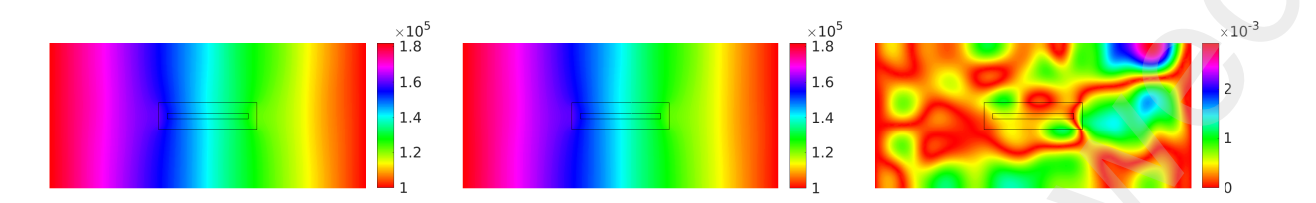


Figure 7: Pressure solution realization (Pa): SFEM (left), MCS (mid) and their relative error (right).

error are depicted in Fig. 7, which verifies the high accuracy of the proposed method for the given sample realization of random inputs. In this sense, the recalculation process using Eq. (31) can be used as a stochastic reduced-order model, allowing real-time or near-real-time simulations for large-scale groundwater systems with uncertainties. Furthermore, in the deterministic solution with homogeneously distributed permeability, a linear pressure gradient is expected from the left to right boundary. However, in our simulation, the introduction of a random field for permeability results in local variations in the pressure field. This highlights the importance of taking uncertainty into account to make the analysis more realistic. These variations will become more prominent when studying the velocity field.

Table 3: Computational times to solve stochastic Darcy flow.

Process	Solving vectors	Recalculation	Total time	MCS
Time	295.89 s	2.60 s	298.49 s	56.73 min

In terms of computational efficiency, as listed in Table 3, the time costs of the proposed method and MCS are 298.49 s and 56.73 min, respectively, which demonstrates that the proposed method is more efficient than MCS by a factor of more than ten. For the proposed method, the computational time consists of the time required to solve for the basis vectors and the recalculation time. The former is the cost from step 2 to step 13 of Algorithm 1, which is 295.89 s in this case. The latter is the cost of the recalculation step 14 of Algorithm 1, which is 2.60 s in this case. The recalculation time is less costly owing to the small size of Eq. (31). Therefore, more sample realizations of the stochastic solution can be solved cheaply if needed.

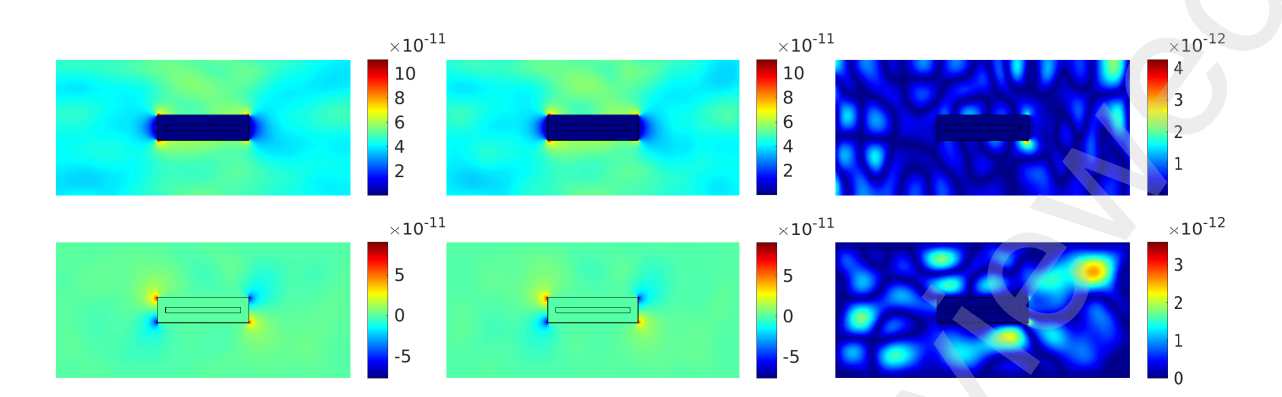


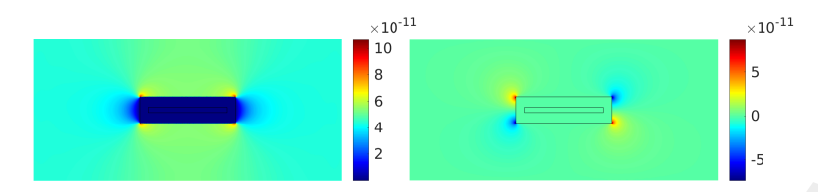
Figure 8: Sample realizations of the stochastic velocity (m/s) in x (top) and z (bottom) directions obtained by SFEM (left), MCS (mid), and their absolute errors (right).

#### 5.3. Results of stochastic velocity and stochastic diffusion-dispersion coefficient propagation

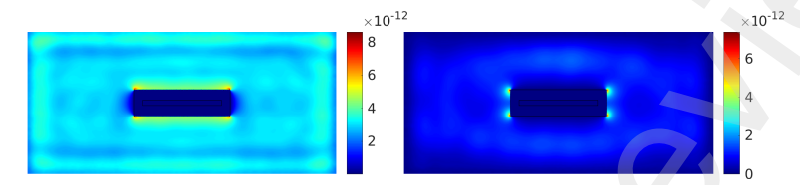
By using Eq. (2) and Algorithm 3, the stochastic velocity can be calculated, where the stopping criterion in step 2 is set to  $\epsilon_q = 1 \cdot 10^{-4}$ . According to Eq. (46), if a direct calculation is used, the stochastic velocity involves  $72 \cdot 35 = 2520$  random variables ( $\xi_j(\theta) \lambda_i(\theta)$ ) is considered as a new random variable), which is reduced to 62 random variables by using Algorithm 3. In terms of approximation accuracy, for a given sample realization, Fig. 8 shows the corresponding sample realizations of stochastic velocities obtained by the proposed method and the direct calculation using MCS. The proposed method is in good agreement with MCS, which verifies the effectiveness of Algorithm 3. Moreover, it can be seen that unlike the symmetric solution in a deterministic analysis, the velocity in the x direction has strong spatial variability, which also leads to non-homogeneous radionuclide migration in space. Furthermore, the stochastic coefficient  $D_p(\theta)$  can be calculated through Eq. (7)

$$\boldsymbol{D}_{p}(\theta) = \begin{bmatrix} D_{p,xx}(\theta) & D_{p,xz}(\theta) \\ D_{p,zx}(\theta) & D_{p,zz}(\theta) \end{bmatrix} = \frac{\alpha_{L} - \alpha_{T}}{\|\boldsymbol{v}(\theta)\|} \begin{bmatrix} v_{x}(\theta) v_{x}(\theta) & v_{x}(\theta) v_{z}(\theta) \\ v_{z}(\theta) v_{x}(\theta) & v_{z}(\theta) v_{z}(\theta) \end{bmatrix} + \alpha_{T} \|\boldsymbol{v}(\theta)\| \boldsymbol{I}_{2}, \quad (53)$$

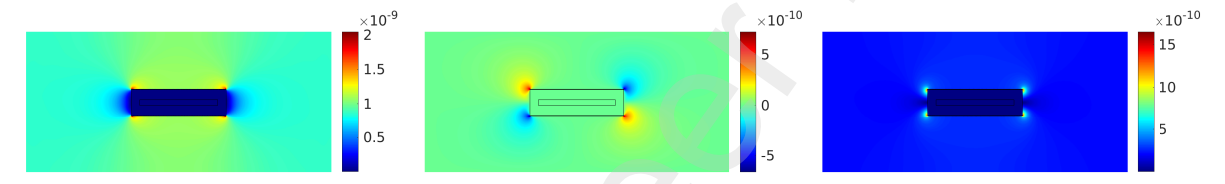
which involves a total of  $2520 \cdot 2520 + 1 = 6350401$  random variables. Algorithm 3 is used to reduce these to 60 random variables. Statistical properties of the velocity vector field, and the dispersivity tensor field are depicted in Fig. 9. The mean values are very similar to the corresponding deterministic analysis. The standard deviations show the random variations of these quantities, which can have significant impacts on subsequent stochastic analysis of radionuclide



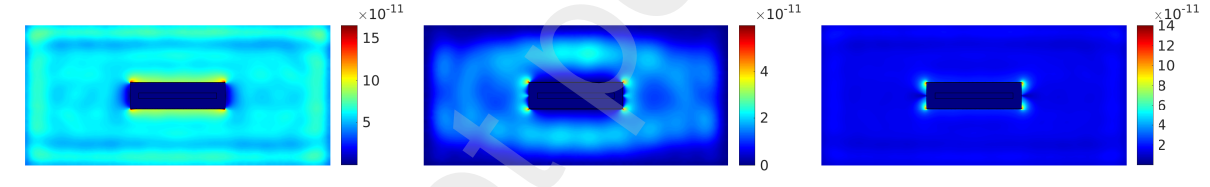
(a) Means of the stochastic velocity (m/s) in x (left) and z (right) directions, respectively.



(b) Standard deviations of the stochastic velocity in x (left) and z (right) directions, respectively.



(c) Means of the stochastic coefficients  $D_{p,xx}(\theta)$  (left),  $D_{p,xz}(\theta)$  (mid) and  $D_{p,zz}(\theta)$  (right), respectively.



(d) Standard deviations of the stochastic coefficients  $D_{p,xx}(\theta)$  (left),  $D_{p,xz}(\theta)$  (mid) and  $D_{p,zz}(\theta)$  (right), respectively.

Figure 9: Means and standard deviations of the stochastic velocity (the first two lines) and the stochastic coefficient  $D(\theta)$  (the last two lines).

mass transport.

### 5.4. Results of stochastic mass transport

For the radionuclide migration process, a total of 122 random variables (62 for velocities and 60 for  $D_p(\theta)$ ) are involved based on the above propagation process. Furthermore, we consider a duration of 1 million years and use a time step of 100 years, thus yielding a total of 10 000 time steps. By using Algorithm 2 to solve Eq. (13), the stopping criterion in step 2 is set to  $\epsilon_C = 1 \cdot 10^{-12}$ , which is used to show that the proposed method can achieve low errors. The iterative errors of

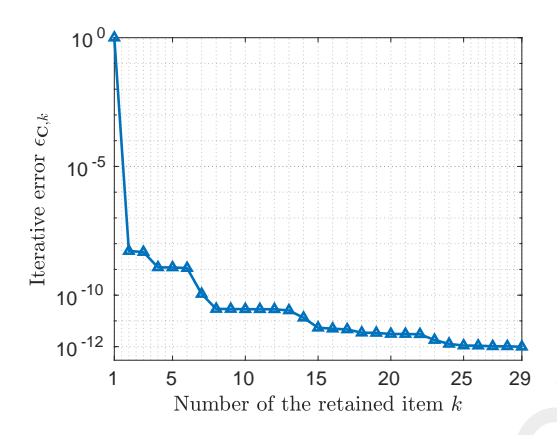


Figure 10: Iterative errors of different retained items.

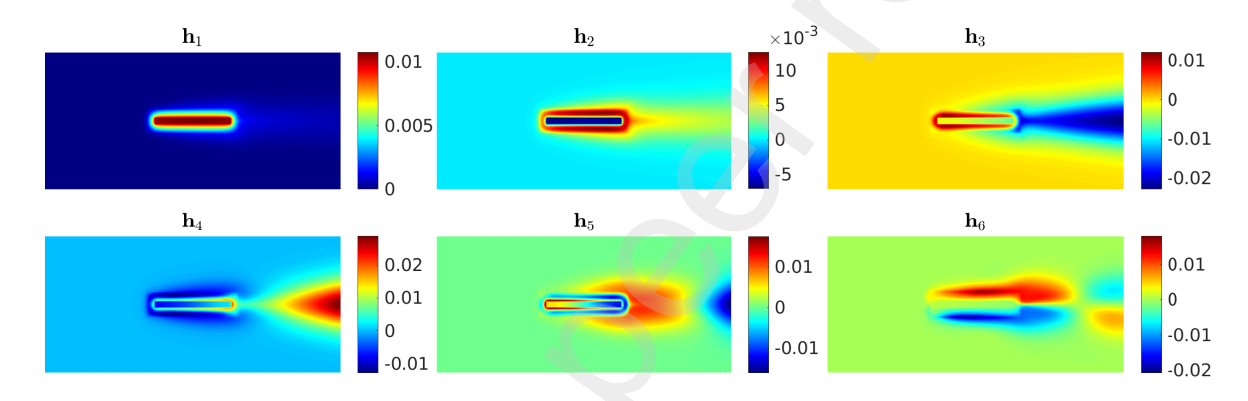
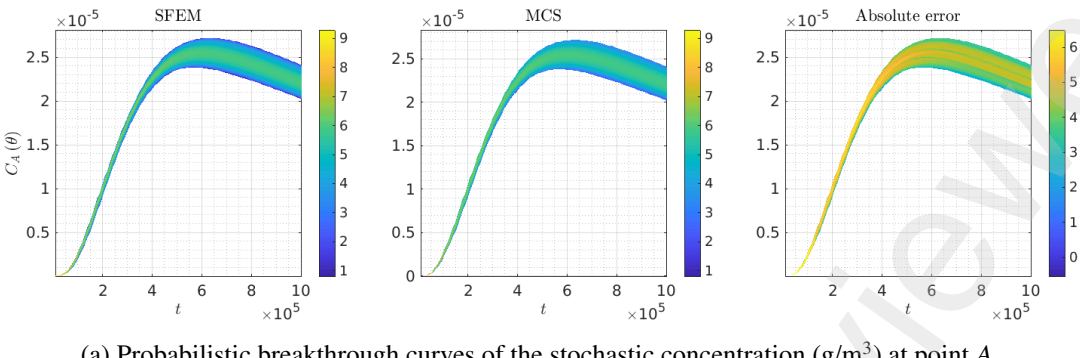


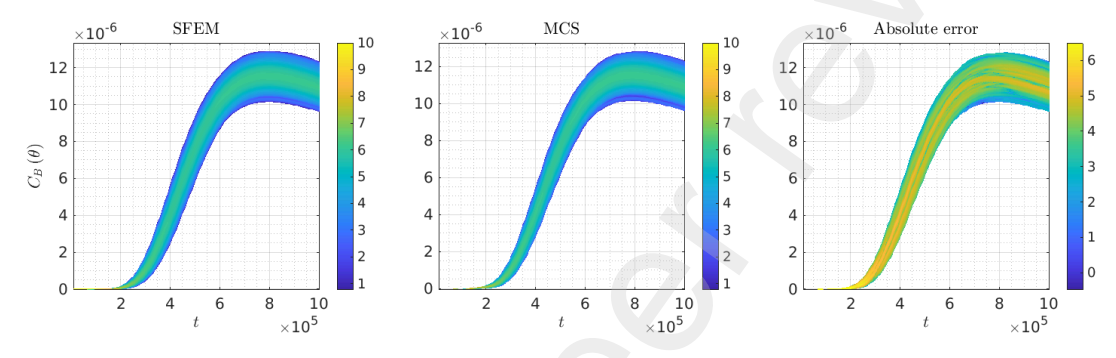
Figure 11: Deterministic vector components  $\{\mathbf{h}_i\}_{i=1}^6$  of the stochastic concentration.

different retained items are shown in Fig. 10. In this case, 29 items are sufficient to achieve the specific accuracy, which demonstrates the good convergence of the proposed method in solving stochastic mass transport. It can be seen that for a stricter stopping criterion, the proposed method can still achieve good convergence and effectively decrease the iterative error. The first six deterministic vectors  $\{\mathbf{h}_i\}_{i=1}^6$  of the stochastic concentration are depicted in Fig. 11, which clearly shows characteristic modes of the radionuclide migration process resembling the source configuration and the near- and far-field plumes.

In terms of computational accuracy, we focus on the probabilistic breakthrough curves at the two reference points A and B (see Fig. 2 left). These breakthrough curves enhanced by evolving PDFs for concentration obtained by Algorithm 2 and MCS, as well as their absolute errors, are depicted in Fig. 12. The proposed method still has an accuracy comparable to that of MCS in



(a) Probabilistic breakthrough curves of the stochastic concentration  $(g/m^3)$  at point A.



(b) Probabilistic breakthrough curves of the stochastic concentration at point B.

Figure 12: Colors indicate the evolution of PDFs of concentration (in decadic logarithmic scale) of the stochastic concentration, providing probabilistic breakthrough curves at reference points A (top) and B (bottom), respectively.

this case. Following groundwater flow and hydrodynamic dispersion, the radionuclides gradually migrate from the emplacement zone to the surrounding regions. Consequently, as shown in our results (Fig. 12), at a given location, the concentration gradually increases over time. After reaching its peak value, the concentration successively decreases as radionuclides are transported to more distant areas. Since the reference point A is closer to the repository, the peak of the concentration is reached earlier, after approximately  $6 \cdot 10^5$  a. In contrast, at the farther point B, the maximum concentration is reached after around  $8 \cdot 10^5$  a. Characterizing the peak concentrations is of critical importance in the context of SA for nuclear waste repositories, as the time of peak release from a CRZ can be regarded as the period of highest risk for the repository. If the containment condition has been ensured in the maximum risk period, long-term safety can usually be guaranteed for the remaining storage period. Typically, long-term SA is recommended to cover up to one million years [43]. National standards for SA timeframes vary from country to country. However, the potential dependency of SA timeframes on the observation regions has been rarely considered. Our results highlight that the time point of peak release is strongly dependent on the boundaries of the CRZ. The results also confirm that the consideration of one million years is reasonable for this study's configuration and can cover periods of peak radionuclide release. In this sense, the proposed stochastic modeling framework could potentially provide reliable guidance to determine the interaction between the timeframes required for safety evaluation and the dimensioning of the CRZ when impacts of uncertainties in radionuclide transport are taken into account.

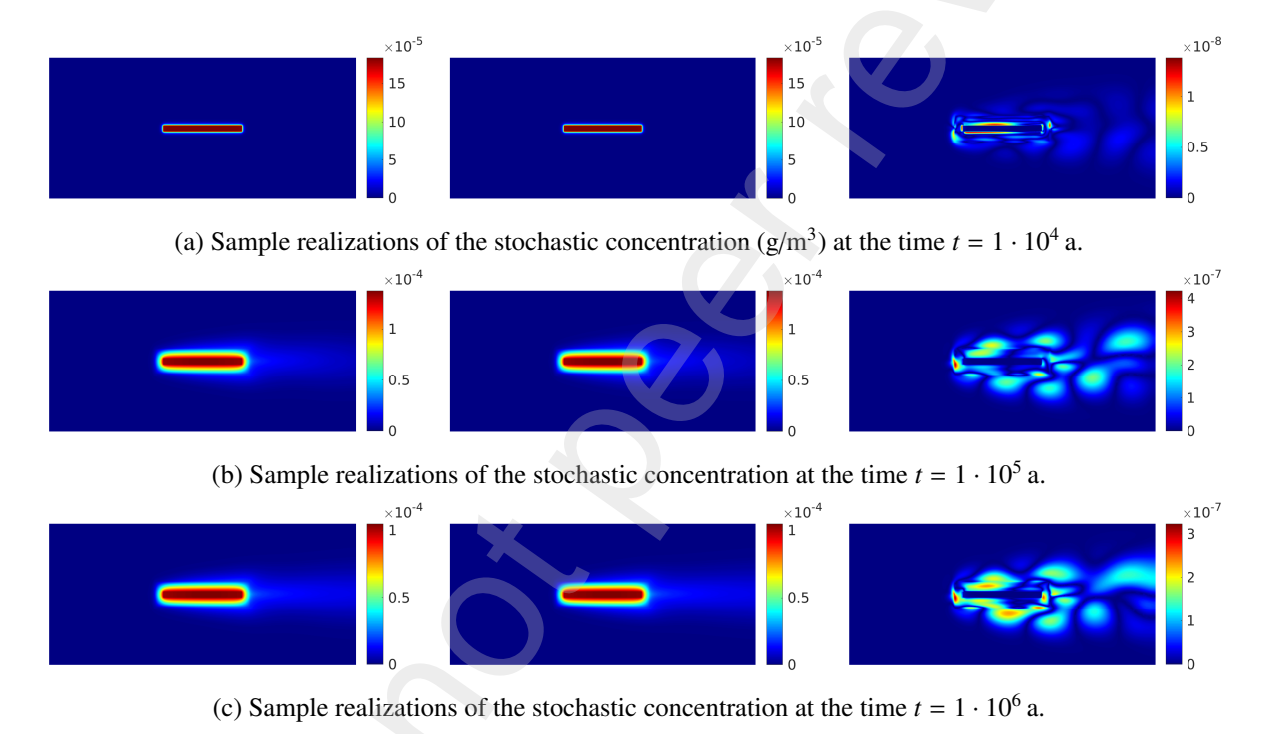


Figure 13: Sample realizations of the stochastic concentration at different times (top to bottom) obtained by SFEM (left) and MCS (mid), and their absolute errors (right).

Also, in addition to probabilistic solutions, we emphasize that the proposed method can accurately solve the sample realization of stochastic concentration corresponding to each sample realization of random inputs. To show this, with a given sample realization of random inputs, the sample realizations of stochastic concentration at different time points obtained by the proposed method and MCS are compared in Fig. 13. The method achieves very small absolute errors, thus verifying the accuracy of Algorithm 2. The method is computationally very efficient for simula-

tions of practically relevant dimensions, i.e. a high number of degrees of freedom and time steps. Computational times of the proposed method and MCS are listed in Table 4, where the vector solution time is the cost from step 2 to step 14 of Algorithm 2 and the recalculation time is the cost of the recalculation step 15. The proposed method is still much more efficient than MCS and achieves a speedup of 170. Furthermore, the recalculation process is performed using the time-parallel solution given in Eq. (41). The computational time is 25.81 s if the non-parallel method in Eq. (39) is used. This also verifies the effectiveness of the proposed time-parallel strategy.

Table 4: Computational times to solve stochastic mass transport.

Process	Solving vectors	Recalculation	Total time	MCS
Time	$1.14 \cdot 10^3 \mathrm{s}$	1.52 s	0.32 h	54.44 h

#### 6. Conclusion

This article developed an effective and efficient framework for handling the influence of uncertainties on radionuclide migration from deep geological repositories. Three challenging aspects are highlighted, including large spatial scales, high-dimensional random inputs, and long durations that require many time steps. The framework relies on the decoupling of stochastic solutions in spatial, temporal and stochastic spaces and dedicated iterative algorithms to solve each component alternately. The effectiveness of the proposed method has been verified using examples with up to 122 random variables, around 60 000 DoFs, and a duration of 1 million years. Furthermore, it was shown that the proposed framework can provide high-accuracy probabilistic transport results in the form of breakthrough curves, thus opening up a powerful pathway for subsequent uncertainty quantification analysis such as reliability-based risk assessment and parameter sensitivity analysis [44, 45], which will be followed up in future studies.

## Acknowledgement

This work was funded by the German Federal Ministry for the Environment, Nature Conservation, Nuclear Safety and Consumer Protection (BMUV) under Grant Number 02 E 12042B within the Christa-III project. The first author is grateful to the German Research Foundation (DFG) project (grant number 527222589) and the Alexander von Humboldt Foundation. The second and third authors acknowledge the professional and administrative support provided by the Project Management Agency Karlsruhe (PTKA). The fourth author acknowledges funding by the Federal Company for Radioactive Waste Disposal (BGE) under Grant Number STAFuE-21-4-Klei as part of the URS cluster.

#### References

- [1] Bundesrepublik Deutschland, Gesetz zur Suche und Auswahl eines Standortes für ein Endlager für hochradioaktive Abfälle (Standortauswahlgesetz StandAG), Bundesgesetzblatt I, 2017, p. 1074, 2017. URL: https://www.gesetze-im-internet.de/standag/, BGBl. I S. 1074, zuletzt geändert durch Artikel 1 des Gesetzes vom 7. Dezember 2020 (BGBl. I S. 2760).
- [2] K. Kurgyis, P. Achtziger-Zupančič, M. Bjorge, M. S. Boxberg, M. Broggi, J. Buchwald, O. G. Ernst, J. Flügge, A. Ganopolski, T. Graf, P. Kortenbruck, J. Kowalski, P. Kreye, P. Kukla, S. Mayr, S. Miro, T. Nagel, W. Nowak, S. Oladyshkin, A. Renz, J. Rienäcker-Burschil, K.-J. Röhlig, O. Sträter, J. Thiedau, F. Wagner, F. Wellmann, M. Wengler, J. Wolf, W. Rühaak, Uncertainties and robustness with regard to the safety of a repository for high-level radioactive waste: introduction of a research initiative, Environmental Earth Sciences 83 (2024) 82.
- [3] S. P. Neuman, Stochastic continuum representation of fractured rock permeability as an alternative to the rev and fracture network concepts, in: ARMA US Rock Mechanics/Geomechanics Symposium, ARMA, 1987, pp. ARMA–87.
- [4] S. P. Neuman, Trends, prospects and challenges in quantifying flow and transport through fractured rocks, Hydrogeology Journal 13 (2005) 124–147.
- [5] C.-F. Tsang, I. Neretnieks, Y. Tsang, Hydrologic issues associated with nuclear waste repositories, Water Resources Research 51 (2015) 6923–6972.
- [6] J.-O. Selroos, D. D. Walker, A. Ström, B. Gylling, S. Follin, Comparison of alternative modelling approaches for groundwater flow in fractured rock, Journal of Hydrology 257 (2002) 174–188.
- [7] X. Zhang, F. Ma, Z. Dai, J. Wang, L. Chen, H. Ling, M. R. Soltanian, Radionuclide transport in multi-scale fractured rocks: A review, Journal of Hazardous Materials 424 (2022) 127550.
- [8] G. Stefanou, The stochastic finite element method: past, present and future, Computer Methods in Applied Mechanics and Engineering 198 (2009) 1031–1051.
- [9] I. G. Graham, F. Y. Kuo, D. Nuyens, R. Scheichl, I. H. Sloan, Quasi-Monte Carlo methods for elliptic PDEs with random coefficients and applications, Journal of Computational Physics 230 (2011) 3668–3694.
- [10] G. Geraci, M. S. Eldred, G. Iaccarino, A multifidelity multilevel Monte Carlo method for uncertainty propa-

- gation in aerospace applications, in: 19th AIAA Non-Deterministic Approaches Conference, AIAA, 2017, p. 1951.
- [11] P. Delgado, V. Kumar, A stochastic galerkin approach to uncertainty quantification in poroelastic media, in: Fluids Engineering Division Summer Meeting, American Society of Mechanical Engineers, 2014, p. V01DT40A002.
- [12] M. Botti, D. A. Di Pietro, O. Le Maître, P. Sochala, Numerical approximation of poroelasticity with random coefficients using Polynomial Chaos and Hybrid High-Order methods, Computer Methods in Applied Mechanics and Engineering 361 (2020) 112736.
- [13] R. Ghanem, P. D. Spanos, Stochastic finite elements: A spectral approach, Courier Corporation (2003).
- [14] D. Xiu, G. E. Karniadakis, The Wiener–Askey polynomial chaos for stochastic differential equations, SIAM Journal on Scientific Computing 24 (2002) 619–644.
- [15] A. Chaudhuri, R. Lam, K. Willcox, Multifidelity uncertainty propagation via adaptive surrogates in coupled multidisciplinary systems, AIAA Journal 56 (2018) 235–249.
- [16] H. Li, C. Liu, A. Saini, Y. Wang, H. Jiang, T. Yang, L. Chen, C. Pan, H. Shen, Coupling multi-physics simulation and response surface methodology for the thermal optimization of ternary prismatic lithium-ion battery, Journal of Power Sources 438 (2019) 226974.
- [17] D. Degen, M. Cacace, F. Wellmann, 3D multi-physics uncertainty quantification using physics-based machine learning, Scientific Reports 12 (2022) 17491.
- [18] O. G. Ernst, B. Sprungk, C. Zhang, Uncertainty modeling and propagation for groundwater flow: a comparative study of surrogates, GEM-International Journal on Geomathematics 15 (2024) 11.
- [19] A. Mittal, X. Chen, C. H. Tong, G. Iaccarino, A flexible uncertainty propagation framework for general multiphysics systems, SIAM/ASA Journal on Uncertainty Quantification 4 (2016) 218–243.
- [20] X. Chen, B. Ng, Y. Sun, C. Tong, A flexible uncertainty quantification method for linearly coupled multi-physics systems, Journal of Computational Physics 248 (2013) 383–401.
- [21] M. Arnst, R. Ghanem, E. Phipps, J. Red-Horse, Reduced chaos expansions with random coefficients in reduced-dimensional stochastic modeling of coupled problems, International Journal for Numerical Methods in Engineering 97 (2014) 352–376.
- [22] P. G. Constantine, E. T. Phipps, T. M. Wildey, Efficient uncertainty propagation for network multiphysics systems, International Journal for Numerical Methods in Engineering 99 (2014) 183–202.
- [23] T. J. Hughes, The finite element method: linear static and dynamic finite element analysis, Courier Corporation, 2003.
- [24] Y. Saad, Iterative methods for sparse linear systems, SIAM, 2003.
- [25] Z. Zheng, M. Valdebenito, M. Beer, U. Nackenhorst, A stochastic finite element scheme for solving partial differential equations defined on random domains, Computer Methods in Applied Mechanics and Engineering

- 405 (2023) 115860.
- [26] Z. Zheng, U. Nackenhorst, Efficient uncertainty propagation for stochastic multiscale linear elasticity, Computer Methods in Applied Mechanics and Engineering 428 (2024) 117085.
- [27] F. Chinesta, R. Keunings, A. Leygue, The proper generalized decomposition for advanced numerical simulations: a primer, Springer, 2013.
- [28] A. Nouy, Proper generalized decompositions and separated representations for the numerical solution of high dimensional stochastic problems, Archives of Computational Methods in Engineering 17 (2010) 403–434.
- [29] M. Jobmann, V. Burlaka, C. Morel Guevara, et al, Methodisches Vorgehen zur sicherheitlichen Bewertung von Endlagersystemen im Kristallin in Deutschland, Synthesebericht BGE TEC 2021-17, BGE TECHNOLOGY GmbH, Peine, 2021.
- [30] E. Simo, P. Herold, M. Jobmann, N. Müller-Hoeppe, M. Gruner, The role of bentonite in the repository concepts for radioactive waste in Germany: a review, Geoenergy 2 (2024).
- [31] C.-H. Lee, B.-W. Deng, J.-L. Chang, A continuum approach for estimating permeability in naturally fractured rocks, Engineering Geology 39 (1995) 71–85.
- [32] S. Sakamoto, R. Ghanem, Polynomial chaos decomposition for the simulation of non-Gaussian nonstationary stochastic processes, Journal of Engineering Mechanics 128 (2002) 190–201.
- [33] K.-K. Phoon, H. Huang, S. T. Quek, Simulation of strongly non-Gaussian processes using Karhunen–Loeve expansion, Probabilistic Engineering Mechanics 20 (2005) 188–198.
- [34] Z. Zheng, M. Beer, U. Nackenhorst, An iterative multi-fidelity scheme for simulating multi-dimensional non-Gaussian random fields, Mechanical Systems and Signal Processing 200 (2023) 110643.
- [35] Z. Zheng, H. Dai, Simulation of multi-dimensional random fields by Karhunen–Loève expansion, Computer Methods in Applied Mechanics and Engineering 324 (2017) 221–247.
- [36] Y. Saad, Numerical methods for large eigenvalue problems, SIAM, 2011.
- [37] P. Hartman, Ordinary differential equations, SIAM, 2002.
- [38] Z. Zheng, M. Beer, H. Dai, U. Nackenhorst, A weak-intrusive stochastic finite element method for stochastic structural dynamics analysis, Computer Methods in Applied Mechanics and Engineering 399 (2022) 115360.
- [39] J. Thiedau, J. Maßmann, C. Guevara More, S. Weihmann, A. Alfarra, CHRISTA-II Analysen zur Integrität von geologischen Barrieren von Endlagersystemen im Kristallin, Ergebnisbericht F+E Endlagerung 9Y2017020000, Bundesanstalt für Geowissenschaften und Rohstoffe (BGR), Hannover, 2021.
- [40] National Cooperative for the Disposal of Radioactive Waste (NAGRA), Wettingen (Switzerland), Project opalinus clay, models, codes and data for safety assessment-demonstration of disposal feasibility for spent fuel, vitrified high-level waste and long-lived intermediate-level waste, Technical Report NTB 02-06, 1015-2636 (2002).
- [41] J. Wolf, D. Becker, J. Flügge, T. Frank, M. Johnen, Bewertung des sicheren Einschlusses von Radionukliden

- in Endlagersystemen im Kristallingestein, Report GRS 658, Gesellschaft für Anlagen und Reaktorsicherheit (GRS) gGmbH, Braunschweig, 2021.
- [42] J. Larue, B. Baltes, H. Fischer, G. Frieling, I. Kock, M. Navarro, H. Seher, Radiologische konsequenzenanalyse, Gesellschaft für Anlagen-und Reaktorsicherheit, 2013.
- [43] IAEA, Disposal of Radioactive Waste, IAEA Safety Standards Series No. SSR-5, International Atomic Energy Agency, Vienna, 2011.
- [44] A. A. Chaudhry, J. Buchwald, T. Nagel, Local and global spatio-temporal sensitivity analysis of thermal consolidation around a point heat source, International Journal of Rock Mechanics and Mining Sciences 139 (2021) 104662.
- [45] J. Buchwald, O. Kolditz, T. Nagel, Design-of-Experiment (DoE) based history matching for probabilistic integrity analysis—A case study of the FE-experiment at Mont Terri, Reliability Engineering & System Safety 244 (2024) 109903.